



Design and engineering heterojunctions for the photoelectrochemical monitoring of environmental pollutants: A review



Lei Shi^a, Yu Yin^{a,b}, Lai-Chang Zhang^a, Shaobin Wang^{c,*}, Mika Sillanpää^d, Hongqi Sun^{a,*}

^a School of Engineering, Edith Cowan University, Joondalup, WA, 6027, Australia

^b School of Environmental and Chemical Engineering, Jiangsu University of Science and Technology, Zhenjiang, 212003, PR China

^c School of Chemical Engineering, The University of Adelaide, Adelaide, SA, 5005, Australia

^d Laboratory of Green Chemistry, School of Engineering Science, Lappeenranta University of Technology, Sammonkatu 12, FI-50130, Mikkeli, Finland

ARTICLE INFO

Keywords:

Semiconductor heterojunction
Visible-light photoelectrochemistry
High-performance determination
Environmental pollution
Heavy metal ions
Organic contaminants

ABSTRACT

Highly toxic pollutants, e.g. heavy metal ions, phenolics, toxins and pesticides, have posed major threats to ecosystem security and public health. It is imperative to develop simple, low cost, sensitive and reliable techniques for detecting these contaminants in the environment. Compared with traditional analytic techniques, photoelectrochemical (PEC) sensing as a newly emerged approach possesses a low background noise and high sensitivity, opening a new platform for rapid and accurate monitoring of the concerned pollutants. The performance of advanced PEC sensors is fundamentally related to the microstructures and configurations of semiconductor-based photoactive nanomaterials. Therefore, a multidisciplinary research effort focusing on the rational design and synthesis of innovative photoactive nanomaterials has recently emerged. This paper provides a comprehensive review on the engineered semiconductors (i.e. doped-semiconductors) and their heterojunctions (e.g. semiconductor-semiconductor, semiconductor-carbon, semiconductor-metal and multicomponent heterojunction) as well as their emerging applications in PEC sensing and monitoring. Particular attention has been paid to various morphologies, e.g. 0D quantum dots (QDs) and nanoparticles (NPs), 1D nanowires (NWS), nanotubes (NTs) and nanorods (NRs), 2D nanosheets (NSs) and 3D aligned arrays, and their effects on the sensing performances. Moreover, the signal response mechanisms and performance evaluations (e.g. sensitivity, linear range, limit of detection, selectivity and stability) of the constructed PEC sensors are discussed. At last, critical challenges and future research perspectives in the fields are proposed.

1. Introduction

The rapid industrialisation and urbanisation in the past few decades have caused increasingly severe environmental pollution, which was already a worldwide issue. A broad range of chemical compounds have been discharged into the environment, for instance, heavy metal ions, toxins, phenolics and pesticides [1,2]. These chemical contaminants have become critical risks to the ecosystem security and public health because of their high toxicity, refractory degradation and easy biological accumulation through the food chain [3,4]. As a consequence, it is highly urgent and desirable to develop simple, inexpensive and highly sensitive methods for the sensing and monitoring of these toxic environmental pollutants.

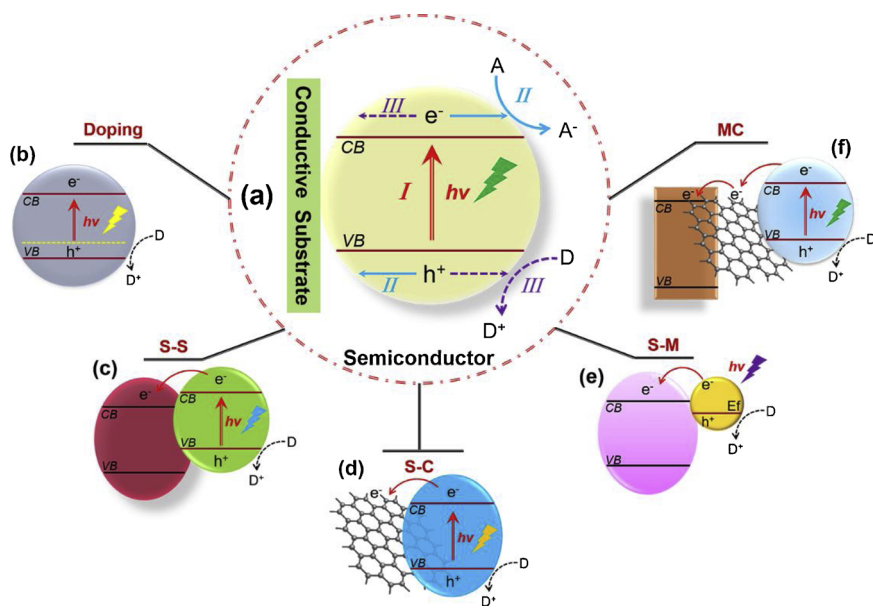
Traditional technologies, for example, inductively coupled plasma mass spectrometry (ICP-MS), atomic absorption/emission spectrometry (AAS/AES), atomic fluorescence spectroscopy (AFS), high performance liquid chromatography (HPLC) coupling with mass spectrometry (MS),

and gas spectrometry (GC), are available for trace analysis of these chemical pollutants. Nevertheless, these methods require large and expensive instruments, sophisticated operation processes and specially trained personnel. Newly emerging photoelectrochemical (PEC) technique, via an innovative integration of light response with electrochemical analysis, has opened a new avenue to attractive analysis for chemical and biological monitoring [5–7]. As light and photocurrent are employed as the excitation source and recognition signal, respectively, a PEC sensor is able to lower the background noise to achieve higher sensitivity than the conventional techniques. Moreover, the utilisation of an electronic readout makes the PEC instrument simple, cost-effective and miniaturised. These salient features make PEC sensors promising candidates for rapid and accurate monitoring of various pollutants.

In a typical PEC sensing procedure, the illumination of a working electrode modified by a photoactive material induces the generation of electron-hole (e-h) pairs (Process I, Fig. 1a). Trapping of the excited electrons on the conduction band (CB) with electron acceptors (A)

* Corresponding authors.

E-mail addresses: shaobin.wang@adelaide.edu.au (S. Wang), h.sun@ecu.edu.au (H. Sun).



would result in the cathodic photocurrent (Process II, Fig. 1a) [8]. Alternatively, the holes on the valence band (VB) transfer to the photoactive material surface and are neutralised by the electron donors (D) at the interface, enabling the electrons to transfer to the electrode and forming the anodic photocurrent (Process III, Fig. 1a). Based on the different formation procedures of the photocurrents at the interfaces, several categories of principles have been involved for PEC sensing. For example, with analytes serving directly as the electron donors or acceptors, feasible PEC assays have been realised via a simple redox strategy [9,10]. Otherwise, utilising a direct chemical reaction or coordination between the targets and photoactive materials [11,12], or an indirect physicochemical interaction between the targets and recognition element (e.g. aptamer, antibody and enzyme) modified photoactive materials [13–15], quantitative response changes in photocurrents are observed and used for effective indication of the concentration of the targets.

In the past few years, the rapid growth of research interests and activities in PEC sensing have been observed. Some reviews have been concentrated on the various directions of PEC analysis (e.g. PEC DNA biosensors, PEC immunoassays and PEC enzymatic biosensors) and their promising applications for the quantitative detection of a variety of analytes [8,16,17]. However, to the best of our knowledge, an integral overview focusing on the PEC monitoring of environmental pollutants has not been available. Specifically, it is noteworthy that the rational design and synthesis of desirable photoactive materials is considered to be one of the most crucial steps to realising a successful PEC assay. Unfortunately, rather few of the previous reviews have paid particular attention to the compositional and morphological diversities of the photoactive nanomaterials towards their PEC sensing performance.

In this review, several typical routes for engineering semiconductors and their derived heterojunctions are firstly introduced. Then, a comprehensive introduction on their recent advances in the accurate, rapid and sensitive PEC monitoring of environmental pollutants is presented. For a better interpretation, different PEC sensors have been classified according to the type of monitoring targets, and each section is subdivided into segments, dealing with the type of sensing strategy. Photoactive materials with different morphologies are emphasised and compared, and their synthetic routes are covered, mainly including the hydrothermal (HT) method, solvothermal (ST) route, electrodeposition approach, anodisation and sol-gel method. Finally, the challenge and prospects for advancing the PEC technique for monitoring environmental pollutants are proposed.

Fig. 1. (a) Schematic illustration of semiconductor-based photocurrent generation: (I) the formation of charge carriers under illumination; (II) the trapping of a CB electron and the formation of cathodic photocurrent; (III) the trapping of a VB hole and the formation of anodic photocurrent. (b) Doped semiconductor. (c) S-S heterojunction. (d) S-C heterojunction. (e) S-M heterojunction. (f) MC heterojunction.

2. Design and engineering semiconductor heterojunctions

On the basis of their favourable band-gap alignment, controllable size and excellent biological compatibility, a wide range of semiconductors, e.g. classical metal oxides of TiO₂ and ZnO, have received enormous interest in the construction of PEC sensors [18,19]. However, the low photo-electron production efficiency due to the short absorption threshold, high e-h recombination rate and the mismatched band structure has severely hindered the feasibility of a single semiconductor. For instance, TiO₂ with a wide band-gap of ~3.2 eV can only be activated by UV or near-UV radiation, which occupies only ~5% of solar energy on Earth. To address these shortcomings, a variety of strategies have been employed to improve the optoelectronic conversion efficiency of a single semiconductor, for example, via heteroatom doping or forming a semiconductor heterojunction.

Doping with another element (e.g. N, Cl and Sn) is an effective strategy to regulate the energy bands of semiconductors [20–22]. Through the formation of Ti-O-N and O-Ti-N, N doping in the crystal lattice of TiO₂ can narrow the band gap energy as well as inhibit the recombination of the photoinduced e-h pairs (Fig. 1b) [23,24]. Therefore, a shift of the absorption edge to a lower energy and a higher conversion efficiency in the visible light region is observed. Another typical doping paradigm of photoactive materials is N doped graphene quantum dots (N-GR QDs) [25,26]. Although pristine GR has a zero bandgap, a bandgap can be effectively engineered into GR QDs due to quantum confinement and edge effects [27,28]. Since N atom has a comparable atomic size and five valence electrons suitable for chemically bonding with carbon atoms, its doping into GR QDs could drastically alter their optoelectronic properties and offer more active sites [29], resulting in enhanced light harvesting, prolonged life time of charge carriers, and much higher photocurrents.

Meanwhile, considerable efforts have been made towards the fabrication of many heterojunctions for improving the optoelectronic conversion efficiencies [30]. Generally, the heterojunctions can be sorted into four categories, (i) semiconductor-semiconductor (S-S) heterojunction. TiO₂/CdSe is an example of the interest, on which the photoexcited electrons created on the CB of CdSe efficiently inject into the CB of TiO₂ (Fig. 1c) [31]. The spatial separation of the e-h pairs in the TiO₂/CdSe interface retards their recombination. Meanwhile, the consumption of the holes on the VB of CdSe by the electron donors facilitates the electron transfer from TiO₂ to the conductive substrate, leading to the generation of an enhanced photocurrent. Apart from familiar metal oxides or chalcogenides, the merging metal-free photoactive materials of GR QDs and carbon QDs (C-QDs) [32,33], or organic molecules of poly(3-

hexylthiophene) (P_3HT) and perylene-3, 4, 9, 10-tetracarboxylic acid (PTCA) [34,35], have also been employed for the creation of versatile heterojunctions. The carbon material-based QDs have shown promising applications in electronic and optoelectronic fields, due to their unique and tunable PEC properties, low toxicity, exceptional biocompatibility and high photostability [36,37]. With regards to the organic molecules possessing impressive semiconductor properties, e.g. large extinction coefficients and high photostability, they could not only absorb broad visible light and offer practical functions as that from sensitizers [38], but also provide favourable processability for the preparation of high-quality heterojunction film [39]. (ii) Semiconductor-carbon (S-C) heterojunction, in which the carbons can be GR [40,41], and its derivatives of graphene oxide (GO) [42], and reduced graphene oxide (rGO) [43], single-walled or multi-walled carbon nanotubes (SWCNTs/MWCNTs) [44,45], and carbon aerogels [46]. For example, due to its excellent electrical conductivity, superior flexibility and extremely high specific surface [47], two-dimensional (2D) planar GR sheet is an ideal supporting scaffold that can be used for homogeneously anchoring of functional nanomaterials [48,49], effectively addressing the issue of easy aggregation. The GR in the heterojunction can promote the charge separation, restrain the e-h recombination as well as provide a large interface for heterogeneous reactions, resulting in a high PEC activity (Fig. 1d) [50]. (iii) Semiconductor-metal (S-M) heterojunction. Au nanoparticles (NPs)/ TiO_2 and Ag NPs/ TiO_2 are well-established examples on which electrons can stay longer in the metal NPs upon charge transfer through the junction interfaces [51,52]. The formation of the Schottky barrier can serve as an efficient electron trap preventing e-h recombination. Particularly, metal NPs with localised surface plasmon resonance (LSPR) or SPR properties are well-known to enhance the visible-light absorption (Fig. 1e) [53,54]. (iv) Multi-component (MC) heterojunction. To simultaneously achieve an enhanced visible light response and transfer of charge carriers, numerous MC heterojunctions consisting of visible-light active components and an electron-transfer system are spatially integrated (Fig. 1f) [55,56]. Attributed to the synergistic effect of CdS (trapping photons from the visible light), rGO (promoting the charge carrier separation and transfer), and ZnO nanowire arrays (NWAs) with a narrowed band gap (collecting the hot electrons form the CdS and rGO), an MC heterojunction of CdS/rGO/ZnO NWAs showed a much better PEC sensing performance [57]. It is found that, through an innovative design and controllable preparation of photoactive materials, significantly enhanced optoelectronic conversion efficiencies have been achieved, offering multiple routes towards construction of high-performance PEC sensors. Table 1 summarises the representative photoactive materials in the PEC monitoring of environmental pollutants. The synthetic method, analysis target, linear range and limit of detection (LOD) in each case are included. The details of the corresponding work can be found in the references cited.

3. PEC based environmental monitoring applications

3.1. Heavy metal ions

Heavy metals are important and toxic pollutants in the environment. They can enter in living organisms through the food chain and cause enzyme inhibition, impaired antioxidant metabolism, DNA damage and depletion of protein sulphhydryl, resulting in severe negative effects on human health [73]. Therefore, the World Health Organization (WHO) has set strict guideline values of heavy metals in drinking water, such as $6\ \mu g\ L^{-1}$ for inorganic Hg, $10\ \mu g\ L^{-1}$ for Pb, $3\ \mu g\ L^{-1}$ for Cd and $50\ \mu g\ L^{-1}$ for total Cr. In the past few years, considerable efforts have been dedicated to constructing sensitive PEC sensors for detecting heavy metal ions. In this section, a systematic introduction on the PEC detection of different heavy metal ions is presented.

3.1.1. Hg^{2+} determination

Zero dimensional quantum dots (0D QDs), also known as colloidal semiconductor nanocrystals, possess unique photophysical properties and

regulated optoelectronic characteristics [74]. These properties enable the wide utilisation of QDs for the fabrication of high-performance PEC sensors [75]. For example, employing dimercaptosuccinic acid (DMSA) capped CdTe QDs fabricated via an electrolysis method, Wen et al. developed a facile PEC sensor for Hg^{2+} detection with a LOD of $0.3\ nM$ [76]. Serving as the trapping sites, the $CdS^{+}-Hg^{+}$ species produced via the reduction of Hg^{2+} on the DMSA-CdTe QDs surface suppressed the formation of the excitons, leading to a quantitative decrease in the photocurrent. With an opposite manner, a signal-on PEC assay for the sensitive detection of Hg^{2+} was realised on 0D HgS/ZnS QDs [77]. Since the formation of an S-S heterojunction facilitated the charge carrier transport and promoted e-h separation, a linearly increased photocurrent was observed for Hg^{2+} in a range of $0.01\text{--}10.0\ \mu M$, and the LOD was determined to be $4.6\ nM$. These studies show facile PEC routes for Hg^{2+} detection. However, in view of the inevitable structure damage of QDs, it should be noted that the potential ion leaching (e.g. Cd^{2+} and Zn^{2+}) would lead to secondary pollution.

Taking the advantages of the tunable LSPR properties of Au@Ag nanorods (NRs) and the monodisperse TiO_2 nanosheets (NSs) with exposure of a high active crystal facet, Zhang et al. developed a simple PEC sensor for Hg^{2+} assay [78]. As revealed in Fig. 2a, the as-synthesised TiO_2 NSs with an average thickness of $\sim 10\ nm$ exhibited a sheet-like nanostructure, and a large percentage of highly reactive (001) planes were observed at their top and bottom facets (Fig. 2b). Since the photocurrent intensity was significantly dependent on the irradiation wavelength, the photocurrent response of Au@Ag NRs/ TiO_2 NSs was explored under the wavelength from 405 to $505\ nm$. Using orange slice-like Au@Ag NRs as the sensitizer (Fig. 2c), a superior photocurrent was achieved at $\sim 430\ nm$ due to a more efficient plasmon-induced charge separation. As the presence of Hg^{2+} inhibited the electron transfer of Au@Ag NRs and quantitatively reduced the photocurrent, the PEC sensor exhibited a linear range from 0.01 to $10\ nM$ (LOD, $2.5\ pM$) for Hg^{2+} detection (Fig. 2d). Attributed to the highly-stable structure of the S-M heterojunction and the absence of biological molecules, this sensor showed a good reproducibility with a relative standard deviation (RSD) of 1.2% ($n = 5$) and excellent storage stability (98%, 3 weeks).

Based on the direct and facile physicochemical interactions between targets and photoactive materials, these proposed PEC sensors achieved acceptable performances in Hg^{2+} determination. In addition to the linear range, LOD and stability, selectivity is another important parameter for the accuracy of PEC sensors. Although these sensors exhibited a good selectivity for Hg^{2+} against most common ions, the presence of Ag^{+} or Cu^{2+} would produce non-negligible interferences. To obtain reliable assay results, additional treatments should be performed to remove these interfering ions prior to PEC tests.

Recently, the introduction of biological recognition molecules, i.e. aptamers, opens a new horizon for designing PEC aptasensors with high selectivity and sensitivity [79]. As a special category of oligonucleotides, aptamers have received enormous interests because of their high specificity and affinity towards a broad range of targets, for example, heavy metal ions, small organic molecules, biological proteins and cells [80–82]. Using CdS QDs-tagged Hg^{2+} aptamer, Ma et al. developed a folding-based PEC aptasensor for Hg^{2+} detection [83]. Consistent with the absorbance features of the CdS QDs, a noticeable photoresponsive signal was observed at $410\ nm$ under the irradiation wavelength from 400 to $600\ nm$, confirming photocurrents originated entirely from the excitation of the QDs. After the formation of thymine- Hg^{2+} -thymine (T- Hg^{2+} -T) duplexes, CdS QDs were drew closely onto the electrode surface, switching on the photocurrent response. As expected, the sensor exhibited a high sensitivity (LOD, $1\ pM$) and an excellent selectivity towards Hg^{2+} even with 200-fold other metal ions (e.g. Zn^{2+} , Pb^{2+} and Cu^{2+}), mainly attributed to the highly specific T- Hg^{2+} -T coordination. In another study, an ultrasensitive PEC Hg^{2+} aptasensor was reported on a heterojunction of PTCA/GO [84]. With an improved separation of photogenerated carriers upon a visible light excitation ($\lambda > 450\ nm$), a significantly enhanced photocurrent (~3.9 times of pristine PTCA) was observed on the heterojunction, owing to the good

Table 1

Representative photoactive materials for the PEC monitoring of environmental pollutants.

Photoactive nanomaterial	Synthetic method	Target	Linear range	LOD	Ref.
Single semiconductor	CdS QDs ^a	Sol-gel	Pb ²⁺ 0.02 nM-2 μM	10 nM 0.01 nM	[58] [59]
	PbS QDs	Sol-gel	Cr ⁶⁺ 0.5-800 nM	0.18 nM	[60]
Doped semiconductor	Co-ZnO NPs ^b	Hydrothermal (HT)	Acetamiprid	0.3 pg mL ⁻¹	[61]
	Mn-Zn ₃ (OH) ₂ V ₂ O ₇ ·2H ₂ O	HT	Aflatoxin B1	0.5 pg mL ⁻¹ -10 ng mL ⁻¹	[62]
S-S heterojunction	CuS NPs/TiO ₂ nanospheres	HT	Microcystin-LR	50 fM-250 nM	[63]
	GL-MoS ₂ /C ₃ N ₄ ^c	Solvothermal (ST)	Cu ²⁺ 0.02-2.0 ng mL ⁻¹	N/A 4.1 pg mL ⁻¹	[64]
S-M heterojunction	CdS QDs/TiO ₂ NTAs ^d	Enzymatic deposition	Asulam	0.02-2.0 ng mL ⁻¹	[65]
	Au NPs/TiO _x nanocavity	Ion sputtering	Kanamycin	2-100 pM	1 pM
S-C heterojunction	Au QDs/CdS NPs	Reflux assembly	Cu ²⁺ 0.5-120 nM	6.73 nM	[66]
	Pd QDs/TiO ₂ NRAs ^e	HT	PCB 101 ^f	0.1 pM-0.5 nM	0.05 pM
MC heterojunction	Bi ₂ WO ₆ /rGO	HT	Pb ²⁺ 0.01-50 μM	3.3 nM	[67]
	BiPO ₄ /rGO	ST	Chlorpyrifos	0.05-80 ng mL ⁻¹	0.02 ng mL ⁻¹
MC heterojunction	TiO ₂ NPs/MWCNTs	Sol-gel	Microcystin-LR	1.0 pM-3.0 nM	[12]
	Ag NPs/TiO ₂ NPs/N-GR	HT	Pb ²⁺ 1 pM-5 nM	0.4 pM	[69]
MC heterojunction	CdSe@ZnS QDs/GR	Layer-by-layer assembly	Paraoxon	1 pM-1 μM	[70]
	ZnO NPs/CdS NPs/GO	HT	Dichlorvos	5 pM-500 pM	10 fM
			Hg ²⁺	1 pM	[71]
			Hg ²⁺	1.5 pM	[72]

^aQDs: Quantum dots; ^bNPs: Nanoparticles; ^cGL-MoS₂/C₃N₄: Graphene-like MoS₂/C₃N₄; ^dNTAs: Nanotube arrays; ^eNRAs: Nanorod arrays; ^fPCB 101: 2,2',4,5,5'-Pentachlorobiphenyl.

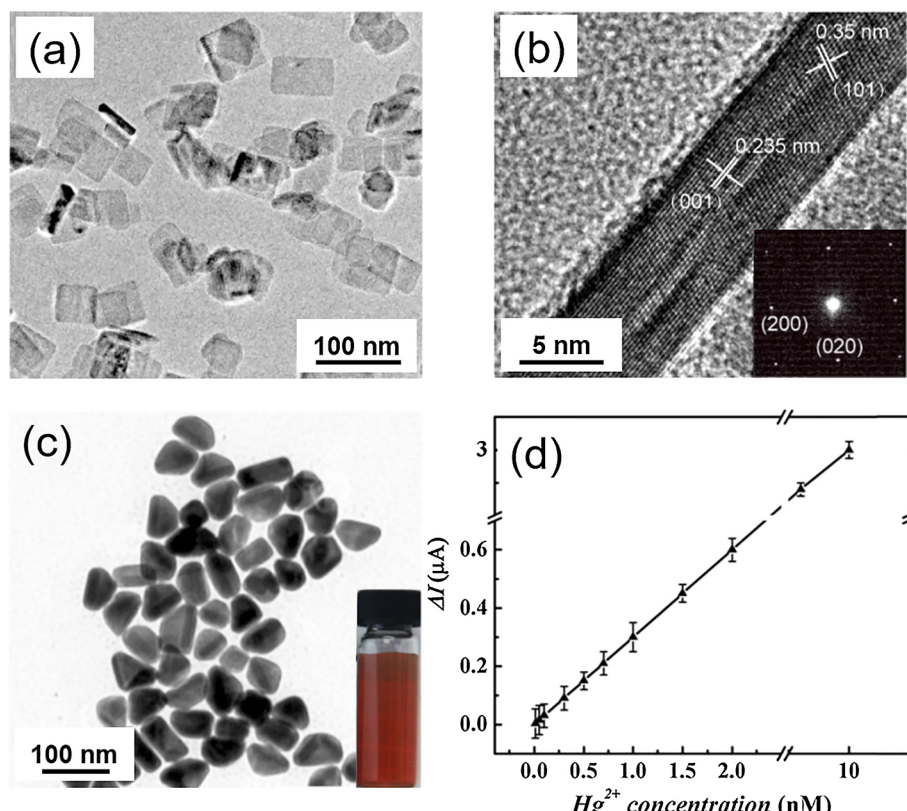


Fig. 2. (a) TEM image, and (b) HRTEM image and crystallographic planes (inset) of TiO₂ NSs. (c) TEM image and photograph (inset) of Au@Ag NRs. (d) Linear calibration curve of photocurrent changes versus Hg²⁺ concentrations [78].

band alignments of n-type PTCA and p-type GO [85]. Since the addition of Hg²⁺ destroyed the poly(dT)-poly(dA) pairings, quercetin-copper complexes serving as both duplex intercalator and electron donor for signal amplification were released from the heterojunction surface, resulting in the decrease of the photocurrents. The prepared sensor possessed an impressively ultralow LOD of 3.33 fM, good specificity and satisfactory recoveries (96.1–107.2%) in tap water, verifying its reliability for real sample monitoring. In addition to a high storage stability (94.7%, 4 weeks), no obvious photocurrent changes in repeated photoexcitation processes (12 times) suggesting that this PEC sensor had a great potential in practical applications.

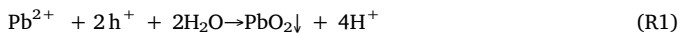
Meanwhile, Li et al. constructed a LSPR-enhanced PEC aptasensor for Hg²⁺ determination based on a PTCA/GR heterojunction and in-situ generated Au NPs via Hg²⁺ specific catalysis [35]. Besides its outstanding optoelectronic property, PTCA can be used to effectively address the agglomeration issue of GR. Therewith, a homogeneous heterojunction interface served as a favourable migration channel for hot electrons generated on Au NPs, resulting in a strong photocurrent. This aptasensor is able to selectively detect Hg²⁺ in a range of 5–500 pM (LOD, 2 pM), and achieves a high storage stability (93.3%, 30 days). In another example of SPR-based PEC aptasensing of Hg²⁺, Shi et al. demonstrated a MC heterojunction of CdSe QDs/Au@Ag NPs/MoS₂ NSs

for achieving an enhanced photocurrent response [86]. Compared with traditional metal oxide semiconductors, MoS₂ NSs possess a layered structure and narrow band gap (~1.9 eV) in the monolayer regime and have great potential applications in nanoelectronics, optoelectronics and flexible devices [87]. Ascribed to a favorable absorbance of constructed heterojunction at the wavelength of 430 nm, a strongest and robust photocurrent response with no noticeable variation in the on/off irradiation cycles (1000s) was obtained at this excitation wavelength. On account of a synergistic effect, a low LOD (5 pM) with excellent selectivity and reproducibility (RSD of 1.87%, n = 5) was achieved on the prepared PEC sensor.

In addition to the SPR effect, the exciton energy transfer (EET) effect amongst Au NPs and various photoactive materials, such as ZnO NPs/CdS NPs/GO [72], CdS QDs [88], and CdS QDs/TiO₂ NPs [89], have been widely observed and utilised for the PEC aptasensing of Hg²⁺. On the basis of the synergistic effect of EET between Au NPs and CdS QDs and sensitisation of rhodamine 123 (Rh 123) for signal amplification, Zhao et al. developed a highly sensitive PEC aptasensor for Hg²⁺ determination [89]. With the incubation of Hg²⁺ disrupted the EET, the photocurrent was recovered and further enhanced with the sensitisation structure. The PEC aptasensor showed an ultralow LOD of 3.3 fM with a wide linear range (10 fM–200 nM), excellent selectivity, and high storage stability with no obvious change in the photocurrent over 2 weeks. Making use of the EET effect, promising PEC sensing systems consisting of Au NPs and versatile heterojunctions are highly anticipated to be designed for monitoring heavy metal ions at low levels.

3.1.2. Pb²⁺ detection

Amongst the various nano-architectures, three-dimensional (3D) aligned arrays consisting of one dimensional (1D) nanotubes (NTs), nanorods (NRs) or nanowires (NWs) possess a fast charge transport through the microscale axial direction, facilitating efficient charge separation across the nanoscale diameters [90–92]. A large specific area would also offer sufficient active sites for the interfacial reactions, and promote the effective acquisition of signals [93]. For example, TiO₂ nanorod arrays (NRAs) prepared by a facile HT route were employed for the PEC sensing of Pb²⁺ [94]. Based on a direct oxidation process (Reaction 1) occurring at the TiO₂ surface, this sensor was used for Pb²⁺ detection at the nanomolar level (LOD, 2 nM). Moreover, via the in-situ electrodeposition of PbS NPs on TiO₂ nanotube arrays (NTAs), Luo et al. fabricated a simple PEC sensor for Pb²⁺ assay [95]. Compared with nanorod structures, hollow nanotubes would provide not only a favourable microenvironment, but much more multidimensional spaces. Accordingly, an increased photocurrent was acquired via the formation of 3D S-S heterojunction, and a LOD of 0.39 nM for selective Pb²⁺ detection was achieved. In view of proposed simple sensing strategies, acceptable assay results were acquired with these Pb²⁺ sensors, confirming the superior properties of 3D array structures in PEC applications.



In the past few years, the successful screening of Pb²⁺-specific aptamer has provided a powerful route to build highly selective assays for Pb²⁺ [96,97]. For example, through Pb²⁺ induced conformation change of G-quadruplex aptamer and subsequent release of hemin, Wang et al. reported a self-operating PEC aptasensor for Pb²⁺ determination on a nanoporous NiO [98]. Since hemin molecules sensitised NiO under the visible light irradiation ($\lambda \geq 400$ nm), the photocurrent increased linearly with Pb²⁺ concentration in the range of 20–1500 nM (LOD, 4.0 nM). Owing to the specific recognition ability of aptamer, the proposed sensor showed a good selectivity for Pb²⁺ against interfering ions of Cd²⁺, Hg²⁺, Cu²⁺, Ag⁺, etc. Taking advantage of a 2D MC heterojunction of Ag NPs/TiO₂ NPs/N-GR prepared via a facile one-pot HT route, Jiang et al. designed a new PEC aptasensor for Pb²⁺ determination [70]. Uniformly dispersed Ag NPs and TiO₂ NPs on the 2D N-GR surface significantly improved the charge transfer rate and lifetime of excitons. Since the

formed G-quadruplex/Pb²⁺ complexes released the quencher at the sensing interface, an ultrasensitive and selective Pb²⁺ assay (LOD, 0.3 pM) with a linear response from 1 pM to 5 nM was achieved. As for the stability, the PEC aptasensor showed robust photocurrent responses in successive 10 tests and remained 93% of the initial response after 3 weeks. To confirm its practical application, the aptasensor was applied in the precise quantifying of Pb²⁺ in tap water with good recoveries (96.6–105.2%). Avoiding complicated procedures usually involved in preparing MC heterojunctions, this work also provides a simple and reliable route for the fabrication of new MC heterojunctions with high PEC activities.

Furthermore, utilising the resonance energy transfer (RET) effect between Au NPs and CdS QDs/rGO NSs, a signal-on PEC aptasensing strategy was designed for Pb²⁺ detection [99]. Comparable with highly dispersed Au NPs with an average size of ~5 nm, enlarged Au NPs assembled with DNA (DNA/Au NPs, ~7 nm in diameter) retained an excellent dispersity (Fig. 3a), which was critical to obtain a robust and sensitive signal response. With CdS QDs homogeneously decorated on rGO NSs (Fig. 3b), this unique 2D heterojunction was demonstrated to be beneficial for the aptamer loading via the π-π interaction and the charge separation. Upon the formation of G-quadruplex/Pb²⁺ complexes, the RET process was disturbed and the recovered photocurrent exhibited a linear response from 0.1 to 50 nM (Fig. 3c). With respect to the selectivity, the sensor showed no noticeable photocurrent change after the addition of interfering ions, e.g. K⁺, Zn²⁺, Co²⁺ and Al³⁺ (Fig. 3d), mainly ascribed to the high affinity of Pb²⁺-specific aptamer.

Possessing a similar recognition function of an aptamer, DNAzyme is another kind of oligonucleotide that is capable of performing a specific catalysis or cleavage reaction in the presence of ions [100–102]. Coupling of Pb²⁺-induced allosteric transition of G-quadruplex DNAzyme and the enzymatic biocatalytic precipitation, a sensitive PEC assay for Pb²⁺ was realised on an S-C heterojunction of Bi₂WO₆/rGO [68]. Bi₂WO₆ has attracted extensive attention in many PEC research fields because of its high stability, suitable band gap (~2.80 eV) and particularly low toxicity compared with inherently toxic CdS and CdSe [103]. The Bi₂WO₆/rGO displayed an enhanced photocurrent intensity (2.7 times of Bi₂WO₆), and stable photocurrent responses under repeated on/off irradiation cycles for 300 s. As anticipated, this sensor showed a sensitive detection of Pb²⁺ at the nanomolar level and achieved a good anti-interference ability. In another study, Zhang et al. proposed a sensitive DNAzyme-based PEC sensor for Pb²⁺ detection (LOD, 0.1 nM) based on a novel 3D ZnO nanoflower [104]. Prepared with a HT decomposition method, the 3D flower-like ZnO consisting of many rod-like nanopetals possessed a high specific area and electron-communication features. Serving as the duplex DNA intercalator and PEC signal reporter [105], the Ru(bpy)₂(dppz)²⁺ (bpy: 2,2'-bipyridine, dppz: dipyrro[3,2-a:2',3'-c]phenazine) was released after the cleavage reaction in the presence of Pb²⁺, resulting in a concomitant photocurrent decrease. On account of the specific recognition ability of DNAzyme towards Pb²⁺, a prominent selectivity was observed with the sensor, even challenging with 100-fold other interfering ions (e.g. Zn²⁺, Cu²⁺ and Cd²⁺).

3.1.3. Cu²⁺ determination

As the third most abundant transition metal in humans, Cu is essential to all living organisms. It serves as a structural and catalytic cofactor for many proteins, and plays an important role in various biological processes. However, excessive ingestion of Cu would cause DNA damages and many neurodegenerative diseases [106]. In addition, a high concentration of Cu²⁺ would depress the self-purification ability of natural waters, since they can kill the biological treatment systems in water.

Owing to a stronger Cu-S interaction than Cd-S and the reduction of Cu²⁺ to Cu⁺ under illumination, the formation of Cu_xS (x = 1, 2) on the CdS surface occurs in the presence of Cu²⁺ via the replacement reaction, generating a lower energy level and providing a path for the recombination of e-h pairs (illustrated in Fig. 4a) [107,108]. Especially, a lower K_{sp} value of CuS than that of PbS, ZnS and other metal sulfides,

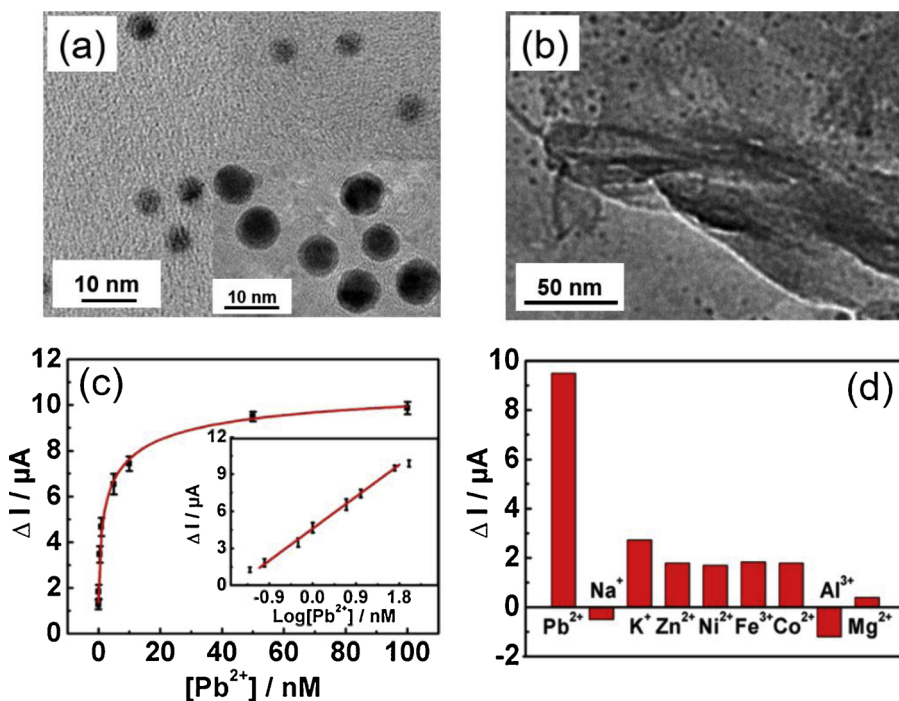


Fig. 3. TEM images of (a) Au NPs and DNA/Au NPs (inset), and (b) CdS QDs/rGO NSs. (c) Photocurrent changes versus Pb^{2+} concentrations. Inset: linear calibration curve. (d) Selectivity test towards Pb^{2+} against other metal ions [99].

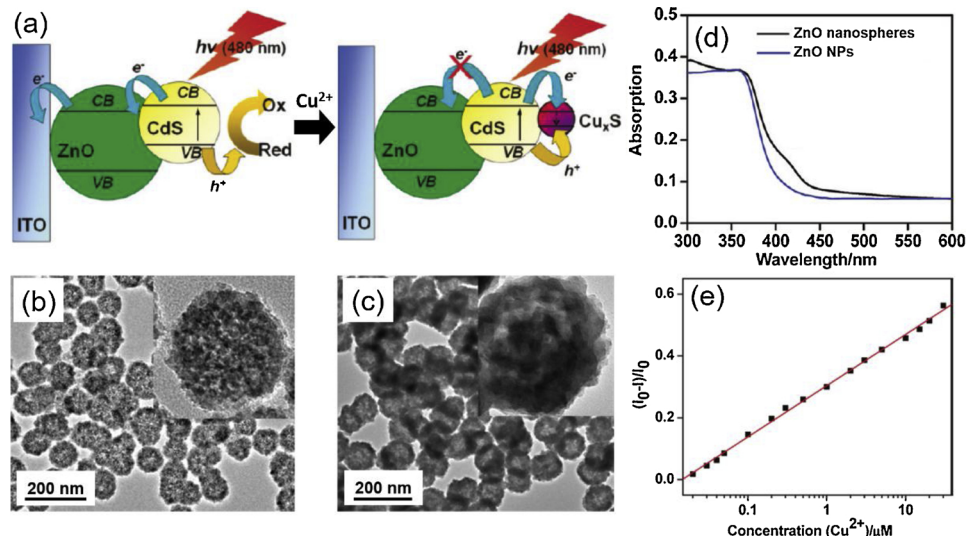


Fig. 4. (a) Photophysics of CdS/ZnO in the absence and presence of Cu^{2+} . TEM images of (b) hierarchical ZnO nanospheres and (c) CdS NPs/ZnO nanospheres. (d) UV-vis absorption spectra of ZnO nanospheres and ZnO NPs. (e) Linear calibration curve of photocurrent changes versus Cu^{2+} concentrations [112].

ensures a satisfactory selectivity for Cu^{2+} detection. Triggered by this replacement strategy, many PEC sensors based on CdS based heterojunctions, such as CdS NPs/SnO₂ [109], CdS NPs/rGO [110], and Cd_{0.5}Zn_{0.5}S NPs/rGO [111] have been designed for the sensitive and selective determination of Cu^{2+} . For instance, hierarchically porous CdS/ZnO nanospheres were fabricated and employed for PEC sensing of Cu^{2+} [112]. Firstly, uniform ZnO nanospheres consisting of plentiful ZnO NPs (~10 nm in diameter) were prepared (Fig. 4b), owing recognisable boundaries and voids between the component subunits. Then, the S–S heterojunction with a unique nano-interface was constructed followed by the selective growth of CdS NPs with a diameter of ~5 nm (Fig. 4c). Compared with the absorption spectrum of ZnO NPs, porous ZnO nanospheres showed an obvious broad absorption peak at ~420 nm, stemming from the light scattering in the presence of larger

secondary colloidal spheres (Fig. 4d). Owing to the highly stable structure of prepared heterojunction, no obvious changes in photocurrents were acquired during successive 30 irradiation tests. Since the photocurrent originated mainly from the excitation of the CdS NPs, an optimal photocurrent response at 480 nm was confirmed during excitation wavelengths from 380 to 540 nm. A significant performance enhancement with a linear range from 0.02 to 40.0 μM (LOD, 10 nM) was observed in Cu^{2+} detection (Fig. 4e). Inspired by this work, Wang et al. prepared hierarchical BiOI microspheres assembled by high-crystalline NSs for the growth of highly dispersed CdS NPs [11]. As a member of bismuth oxyhalides (BiOX, X = Cl, Br and I) possessing excellent photocatalytic activities, BiOI has the strongest absorption in the visible light region due to its favourable band gap (~1.75 eV) [113]. Although photocurrents declined with increasing exciting wavelengths

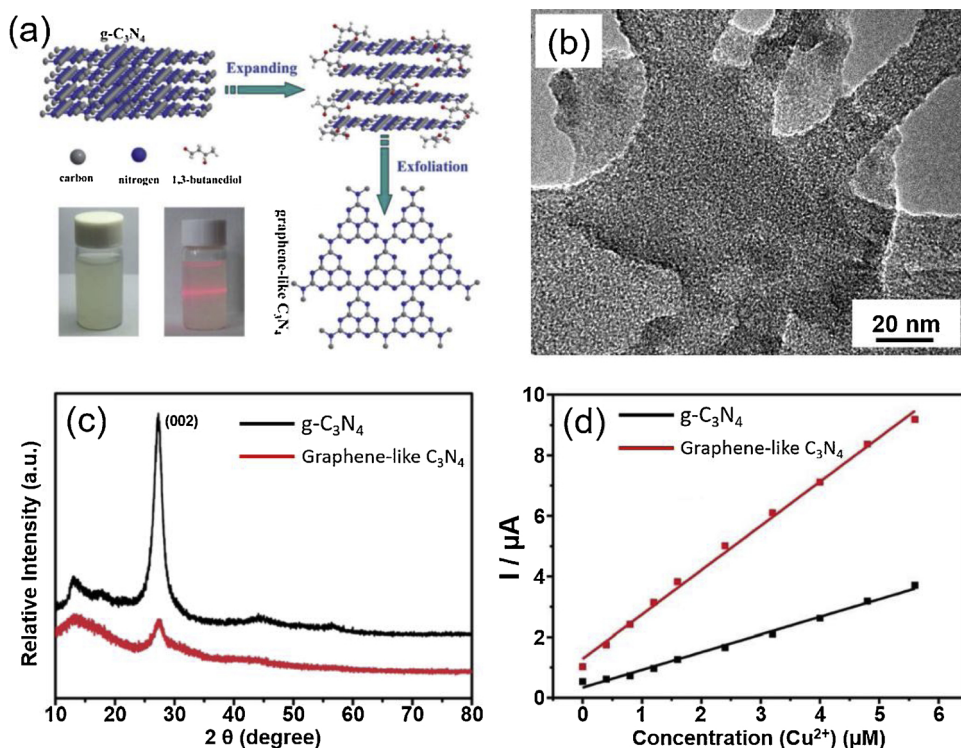


Fig. 5. (a) Schematic illustration for the preparation of graphene-like C₃N₄. (b) TEM image of the graphene-like C₃N₄. (c) XRD patterns of the graphene-like C₃N₄ and g-C₃N₄. (d) Linear calibration curves of photocurrents versus Cu²⁺ concentrations [124].

(430–580 nm), rapid photocurrent decays were observed at low wavelengths because of the rapid recombination of the e–h pairs. Therefore, an optimal 470 nm was chosen to achieve a robust and sensitive photocurrent. The PEC sensor showed a significantly enhanced photocurrent for Cu²⁺ determination (LOD, 20 nM), as well as high selectivity and storage ability (94.4%, 2 weeks). However, despite its advantage, the replacement strategy usually suffers from two limitations of (i) poor repeatability and (ii) secondary pollution, due to the structure damage of CdS and accompanying Cd²⁺ leaching.

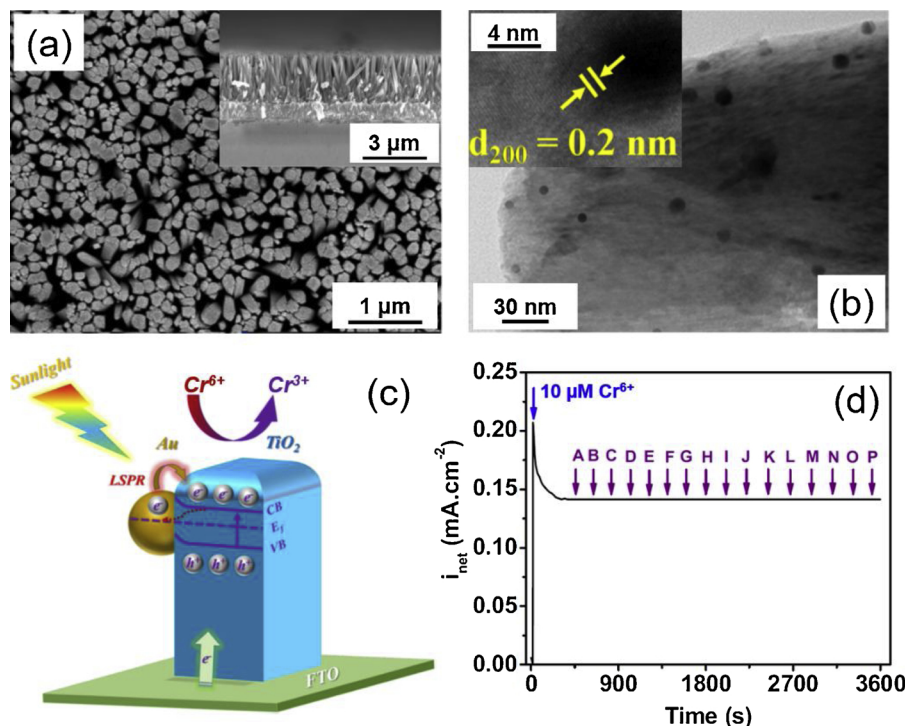
Instead of the replacement strategy, Qiu et al. reported a facile PEC sensor for Cu²⁺ detection via the in-situ electrodeposition of cubic Cu₂O [114]. With enhanced photocurrents produced at a high Cu²⁺ concentration, the proposed PEC sensor showed a wide linear range (10 pM–1 mM) with an ultralow LOD of 3.33 pM. The prepared PEC sensor was successfully applied for Cu²⁺ detection in river water samples with recoveries between 96.6–106.3%. Via selecting a proper electrodeposition potential, the sensor displayed a good selectivity towards most common ions, such as 1000-fold Fe³⁺, 100-fold Sn²⁺, 50-fold Pb²⁺ and Cd²⁺, etc. Nevertheless, a high concentration Cl⁻ (8-fold) severely affected its accuracy, because the adsorbed Cl⁻ on the different planes of cuprous changed the Cu₂O morphology. In addition to its impressive performance for Cu²⁺ assay, the produced Cu₂O could be further modified and applied for PEC sensing of other important biological analytes, e.g. glutathione [115], L-Cysteine [116] and glucose [117].

In recent years, functional C₃N₄ with various morphologies has attracted a great deal of scientific interests in catalysis, sensing and bio-imaging applications [118–121], owing to its unique electronic, surface and optical properties. Compared with bulk C₃N₄, an excellent PEC activity of highly anisotropic C₃N₄ NSs could benefit from: (i) an enhanced absorption of light intensity and extension of absorption range, (ii) more active and adsorption sites provided by a high specific surface area, (iii) strikingly improved electron transport ability along the in-plane direction, and (iv) an increased lifetime of photoexcited charge carriers due to the quantum confinement effect [122,123]. For instance, treating with liquid exfoliation in 1,3-butanediol, graphene-like C₃N₄ was firstly synthesised from the bulk graphitic C₃N₄ (g-C₃N₄) (Fig. 5a) [124]. 2D

graphene-like C₃N₄ possessed a thin-layer and transparent structure (3–6 atom thickness, Fig. 5b), high specific surface area ($\sim 32.54 \text{ m}^2 \text{ g}^{-1}$), and improved electron transport ability. Moreover, a significantly decreased intensity of the (002) peak further proved the successful exfoliation of bulk g-C₃N₄ (Fig. 5c). As Cu²⁺ consumed photoexcited electron from graphene-like C₃N₄ and was reduced on Pt electrode, gradually increased photocurrent was observed at a high Cu²⁺ concentration, resulting in a higher sensitivity than that of g-C₃N₄ (Fig. 5d). Moreover, through hydrothermally treating bulk g-C₃N₄ using NH₄Cl, novel g-C₃N₄ nanorods were synthesized for PEC Cu²⁺ determination with the same sensing strategy [125]. Owing to enhanced light absorption, charge separation and ionic conductivity, obviously increased photocurrent intensity was observed on g-C₃N₄ nanorods (~ 2 times of g-C₃N₄) and a high sensitivity for Cu²⁺ detection with a wide range from 0.018 to 55 μM (LOD, 6.2 nM) was achieved. Even compared with graphene-like C₃N₄, a superior assay performance was observed with g-C₃N₄ nanorods, mainly attributed to that 3D structure of nanorods supplied sufficient active sites and provided favourable mass-transfer profile at the interface. As revealed in these researches, it is confirmed the morphology regulation of photoactive materials plays a critical role in their PEC activity. As for selectivity, undesired signals may be generated with other metal ions (e.g. Ag⁺, Co²⁺, Fe³⁺ and Pb²⁺) due to their potential reduction on the Pt electrode. It is a common issue in such PEC sensors without the usage of recognition elements, and enormous efforts are urgently required to improve their selectivity in future work. Apart from the sensing application, it is noteworthy that these researches also provide a great potential to realise the recovery of valuable Cu²⁺ from wastewater via the utilisation of green solar energy.

3.1.4. Cr⁶⁺ assay

Cr³⁺ and Cr⁶⁺ are the two prominent stable species of Cr ions in the environment, and the transformation between them strongly depends on the solution pH and oxidative properties of the location [126]. With a comparison of Cr³⁺, Cr⁶⁺ is certainly toxic and carcinogenic for humans with severe health hazards. For this reason, reliable and accurate Cr⁶⁺ detection in the environment is of critical importance.



Utilising a competitive redox reaction between Cr⁶⁺ and quercetin, Li et al. reported a PEC sensor for Cr⁶⁺ based on TiO₂ NPs [127]. As the quercetin was served as both electron donor and photosensitiser, the occurred redox reaction quantitatively inhibited the photocurrent response. Under the optimum conditions, the sensor displayed two linear ranges (1–10 nM and 20–140 nM) with a LOD of 0.24 nM.

Recently, Moakhar et al. reported PEC sensors for Cr⁶⁺ determination with Au NPs decorated screen-printed TiO₂ NPs and TiO₂ NRAs [128,129]. Highly oriented TiO₂ NRAs with an average diameter of ~150 nm and thickness of ~2.8 μm were prepared with a facile HT method (Fig. 6a) [128]. Treating with an electrodeposition approach, Au NPs with a diameter of ~10 nm were homogeneously dispersed on the 3D TiO₂ NRAs (Fig. 6b). Upon the irradiation of sunlight, hot electrons generated in Au NPs on the basis of LSPR effect can tunnel into the CB of TiO₂. Simultaneously, photogenerated electrons in TiO₂ were excited to the CB, leaving positively charged holes in the VB. These electrons were consumed on the heterojunction interface, realising the reduction of Cr⁶⁺ into Cr³⁺ (Fig. 6c). Accordingly, the prepared PEC sensor exhibited a high sensitivity of 13.94 μA μM⁻¹ towards Cr⁶⁺ detection (LOD, 6 nM). Notably, this sensor showed no observable responses even being challenged with a wide range of interfering ions at high concentrations (Fig. 6d), demonstrating an excellent anti-interference ability. Attributed to the highly stable structure of produced heterojunction, steady photocurrent responses in 100 continuous tests as well as superb repeatability (RSD of 1.5%, n = 20) and storage stability (96%, 3 months) were observed. While testing with a similar heterojunction of Au NPs/TiO₂ NPs at the same condition [129], a lower sensitivity of 11.88 μA μM⁻¹ was observed in the Cr⁶⁺ determination. This result demonstrated the merits of 3D array structures in the PEC sensing applications, owing to their beneficial electron transfer, efficient separation of charge carriers, and facilitated mass transfer.

Molecular/ion imprinting technique is a promising approach to improve the assay specificity, via the creation of tailor-made binding sites with memory of the shape, size and functional groups of the template molecules/ions [130–132]. Accordingly, various molecularly/ion imprinted polymers (MIPs/IIPs) have aroused extensive attention on account of their desired selectivity, physical robustness and easy preparation [133]. Utilising the formate anion incorporated g-C₃N₄ smartly

Fig. 6. (a) Top and cross-sectional (inset) SEM images of Au NPs/TiO₂ NRAs. (b) TEM and HRTEM (inset) images of Au NPs on TiO₂. (c) Schematic mechanism for PEC sensing of Cr⁶⁺. (d) Selectivity test of PEC sensor (from A to P: 10 mM Cr³⁺, 4 mM Fe³⁺, K⁺, Mg²⁺, Ca²⁺, Zn²⁺, Pb²⁺, Hg²⁺, Cd²⁺, NO₃⁻, Cl⁻, S₂O₃²⁻, VO₃⁻, MnO₄⁻, MoO₄²⁻ and WO₄²⁻). [128].

integrated with an IIP of Cr⁶⁺, Fang et al. developed a rapid and highly sensitive PEC method for the determination of Cr⁶⁺ in water samples under visible-light irradiation ($\lambda = 420$ nm) [134]. Accompanying with an efficient reduction towards Cr⁶⁺ with photogenerated electrons, the PEC analysis was highly linear with Cr⁶⁺ concentrations from 0.01 to 100.0 μg L⁻¹ (LOD, 6.0 ng L⁻¹) with a good storage stability (96%, 30 days). The sensor showed negligible photocurrent changes (< 3.0%) towards non-specific ions, except for Cu²⁺ and Fe³⁺ due to their more positive redox potentials. To exclude such interferences, EDTA was suggested as an efficient masking reagent. In view of doping formate anions into the in-plane holes of C₃N₄ obviously suppressed the recombination of e-h pairs, this work offered an alternative approach for effectively engineering g-C₃N₄ to boost its PEC activity.

3.1.5. Cd²⁺ monitoring

Besides the above mentioned metal ions, some efforts have been dedicated to the construction of PEC sensors for Cd²⁺ detection recently. Through an in-situ electrodeposition of CdSe clusters on 3D TiO₂ NTAs, Liang et al. firstly reported a facile PEC approach for Cd²⁺ determination with a high selectivity and sensitivity [135]. This unique heterojunction exhibited a high incident photo to current efficiency (IPCE) of ~9.5% at a wavelength of ~540 nm, which was in a good agreement with the UV-vis absorption spectrum. This observation confirmed that the produced photocurrents were ascribed to CdSe clusters generated on the TiO₂ NTAs. With enhanced absorption peaks in the visible region due to the formation of CdSe with a narrow band gap (~1.76 eV), linearly increased photocurrents in a very broad linear range (1 nM - 10 mM) were recorded. The LOD of 0.35 nM was far lower than the standard required by the WHO in drinking water. Due to the special formation of CdSe in the presence of SeO₂, negligible effects on the signals (< 3%) of common interfering ions were observed for Cd²⁺ sensing. Stimulated by this work, several sensitive assays of Cd²⁺ were realised via the formation of CdS/ZnO NRAs (LOD, 3.3 μM) and Zn doped CdS film (LOD, 0.35 nM) with the electrodeposition method [136,137].

These pioneering researches not only paved a new way for the PEC determination of Cd²⁺, but also established a facile route to convert heavy metal ions into useful photoactive materials. Particularly, the CdS based photoactive nanomaterials could be further used for other

PEC sensing applications, e.g. Cu^{2+} detection, realising multifunctional assays with constructed PEC sensors.

3.1.6. Perspectives

Evidently, enormous efforts and advances have been made to design and develop applicable heterojunctions for the PEC detection of heavy metal ions. Significantly improved sensing performance, specifically in terms of a high sensitivity, wide linear range and low LOD, has been achieved. Through introducing diverse recognition elements of aptamer, DNAzyme and IIP, a satisfactory selectivity is realised with constructed PEC sensors. Despite this impressive progress in the last few years, some challenges remaining on the heterojunctions in research need to be addressed for advanced PEC sensors in future applications, including (i) tedious preparation procedure, (ii) insufficient electrical conductivity, (iii) poorly controllable morphology, and (iv) weak structural stability. For example, although CdS has been widely used for the PEC detection of Hg^{2+} , Pb^{2+} and Cu^{2+} , the photo-corrosion issue would definitely reduce its optoelectronic conversion efficiency and long-term stability for the generation of a PEC signal. In addition, an in-depth exploration towards electron transfer paths at various interfaces and physicochemical interactions between target ions and heterojunctions are imperative to optimize their structure, composition and morphology. Moreover, in addition to their sensing functionality, promising heterojunctions capable of simultaneous removal of these toxic metal ions seem to be of great significance. These advances would be beneficial to design highly efficient heterojunctions in PEC sensors for heavy metal ions.

3.2. Organic pollutants

3.2.1. Pesticides

Pesticides, for instance organophosphate pesticides (OPs), are widely used in agriculture and as nerve agents of chemical and biological warfare agents. It has been known that OPs are the most toxic species posing rapid and severe effects on human and animal health, resulting from their ability to block the activity of acetylcholinesterase (AChE), a critical central-nervous-system enzyme [138]. In the past few years, many photoactive nanomaterials have been employed for constructing PEC sensors in the detection of pesticides (Table 2).

Serving as the sacrificial agent to consume the hydroxyl radical produced by the photoinduced holes, a sensitive PEC sensor for the chlorpyrifos (CPF) detection was achieved on the heterojunction of poly(3-hexylthiophene) (P3HT)/ TiO_2 NPs [139]. In addition to an excellent absorption in visible region and charge carrier mobility, P3HT possessed a high processability and long-term stability, demonstrated to be a reliable candidate as a sensitiser and protective agent for TiO_2 NPs. In consequence, a high sensitivity (LOD, 10 nM) and storage stability (95.3%, 4 weeks) were achieved in CPF detection. Except for the hydrolysis product (chlorpyrifos oxon and trichloropyridinol) of CPF, the PEC sensor possessed an excellent specificity against other common pesticides.

Table 2
Photoactive nanomaterials based PEC monitoring of pesticides in environmental samples.

Photoactive nanomaterial	Recognition element	Target	Linear range	LOD	Real sample	Ref.
TiO_2 NPs	N/A	Dichlofenthion	0.02–0.1 μM ; 0.2–1.0 μM	2.0 nM	Vegetable extract	[140]
$\text{BiOBr}/\text{N-GR}$		Chlorpyrifos (CPF)	5 pg mL^{-1} –11.6 ng mL^{-1}	1.67 pg mL^{-1}	Vegetable extract	[141]
I-BiOCl/N-GR QDs		CPF	0.3–80 ng mL^{-1}	0.01 ng mL^{-1}	River water	[142]
PTCA/ TiO_2 NPs		Parathion methyl	0.1–10 nM	0.08 nM	Vegetable extract	[143]
$\text{Cd}_{0.5}\text{Zn}_{0.5}\text{S}/\text{rGO}$	AChE	Dursban	0.001–1 $\mu\text{g mL}^{-1}$	0.3 ng mL^{-1}	Tap/River water	[144]
GR QDs/CuFe ₂ O ₄		CPF	0.001–1 $\mu\text{g mL}^{-1}$	0.3 ng mL^{-1}	River water	[145]
$(\text{TAA})_2/\text{TiO}_2$ NPs ^a	MIP	Parathion	2 pg mL^{-1} –4 $\mu\text{g mL}^{-1}$	0.56 pg mL^{-1}	Juice	[146]
$\text{PoPD}/\text{Au NPs}/\text{TiO}_2$ NTAs ^b		CPF	0.05–10 μM	0.96 nM	Vegetable extract	[147]
$\text{TiO}_2/\text{Carbon aerogel}$		Atrazine	0.12–93 μM	8.0 nM	Surface water	[148]
$\text{Au NPs}/\text{CdTe QDs}$		S-fenvalerate	10 nM–1 μM	3.5 nM	Fruit/Vegetable extract	[149]
tS-GR/ZnO nanoplate ^c	Aptamer	Acetamiprid	1–1000 ng mL^{-1}	0.33 ng mL^{-1}	Vegetable extract	[150]
CdTe QDs/MWCNTs/rGO		Acetamiprid	0.5 pM–10 μM	0.2 pM	Fruit extract	[151]

^aT(TA)₂: di-branched di-anchoring dye of triphenylamine derivative; ^bPoPD: poly(o-phenylenediamine); ^ct-S-GR: thiophene-sulfur doped graphene.

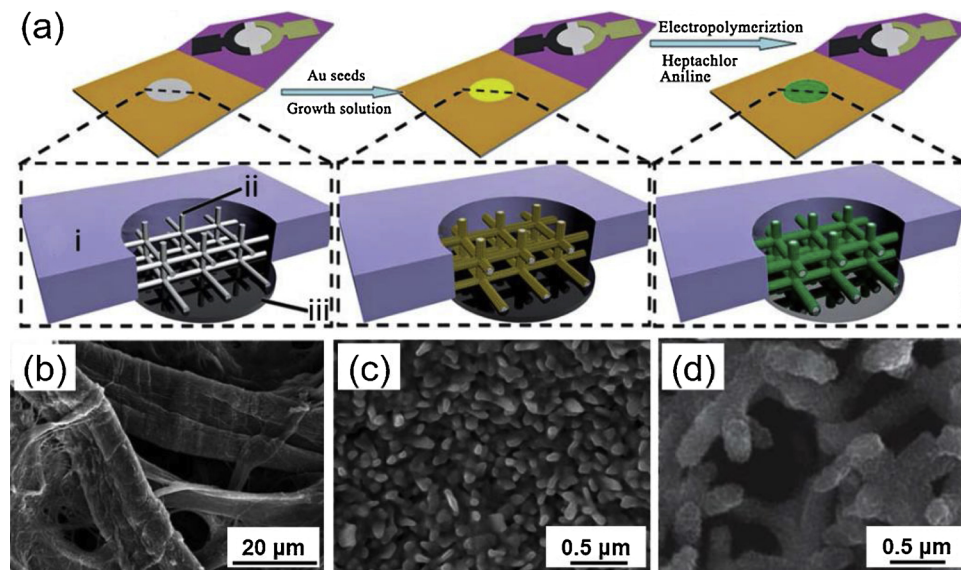


Fig. 7. (a) Schematic fabrication procedures for the disposable microfluidic PEC origami device, (i) wax-penetrated paper, (ii) porous paper sample zone, (iii) screen-printed carbon electrode. SEM images of (b) bare paper sample zone of the PWE, (c) Au NPs on the surface of cellulose fibres and (d) MPANI fibres on the AuNPs-coated cellulose fibres [158].

constructed a sensitive PEC sensor for CPF detection based on a MIP-modified 3D hierarchical branched TiO₂ (B-TiO₂) NRAs [156]. Compared with smooth TiO₂ NRAs, B-TiO₂ NRAs showed excellent light-trapping characteristics, highly conductive pathway for charge collection, and a large surface area for MIP loading [157]. As captured CPF molecules hindered the light harvesting and electron transfer, the photocurrent response was inversely proportional to the CPF concentration in a linear range from 0.01 to 100 ng mL⁻¹ (LOD, 7.4 pg mL⁻¹). Besides, the sensor possessed a satisfied long-term storage stability (90.64%, 30 days) and excellent specificity towards other interfering analogues, e.g. parathion methyl, fenitrothion and triazophos. Stimulated by the enormous demands in the practical applications, Wang et al. proposed a low-cost, simple and portable PEC device for the detection of heptachlor, based on the molecular imprinted polyaniline (MPANI) coupling with a novel Au NPs-modified paper working electrode (Au-PWE, Fig. 7a) [149,158,159]. As shown in Fig. 7b, 3D porous PWE consisting of interlaced cellulose fibres possessed a high specific area ($9.5 \text{ m}^2 \text{ g}^{-1}$), offering a favourable microenvironment for the growth of continuous and dense Au NPs (Fig. 7c). Tangled MPANI fibres (~150 nm in diameter) with porous networks on the Au-PWE supplied sufficient binding sites for heptachlor recognition (Fig. 7d). In view of the photocurrent was originated from the MPANI fibres instead of the AuNPs, the highest photocurrent response was observed at 420 nm during the excitation wavelengths from 400 to 540 nm. As the specially captured heptachlor hindered the diffusion of electron donor, the photocurrent decreased over a wide concentration range from 0.03 to 10 nM, and a LOD of 8.0 pM was calculated with developed sensor. Inspired by this successful paradigm, a prosperous development on microfluidic PEC analytical origami devices decorated with diverse photoactive heterojunctions will be highly anticipated in the future.

Apart from its intrinsic optoelectronic property, multifunctional 2D MoS₂ has also been demonstrated as an excellent supporting matrix for decorating functional nanomaterials [160,161]. Comparable with 2D ultrathin C₃N₄ NSs discussed previously, few-layer MoS₂ play a deterministic role in its PEC activity due to the strong photoresponse, high in-plane electron mobility and large current carrying capacity [162,163]. As practice, Jiang et al. designed a 2D heterojunction of N–GR QDs/MoS₂ NSs via the HT method, and proposed a new insight towards the charge-separation mechanism in the PEC aptasensing of acetamiprid [164]. Well-defined and plate-like MoS₂ possessed obvious ripples and corrugations, revealing the ultrathin nature of the produced MoS₂ (Fig. 8a). After coupling with N–GR QDs, numerous dark dots (~3 nm in diameter) were homogeneously dispersed on the MoS₂ NSs, forming a superior and intact heterointerface (Fig. 8b). As anticipated, the N–GR

QDs/MoS₂ displayed slow decay kinetics in contrast to pristine MoS₂ and achieved a longer lifetime of charge carriers (~3.25 s) than that of MoS₂ (~1.03 s, Fig. 8c), realising a lower recombination rate of e–h pairs and a higher PEC response. With captured acetamiprid prevented the transfer of photogenerated electrons, photocurrent decreased linearly from 0.05 pM to 1 nM (Fig. 8d). An ultralow LOD of 16.7 fM as well as a high selectivity and storage stability with no significant change in photocurrent over 2 weeks was realised. Inspiringly, via exploring and revealing the charge-separation mechanism at the heterointerface, it will provide a guidance on the design and preparation of highly-efficient photoactive materials. Other PEC aptasensors for pesticide determination were constructed on the Co-ZnO diluted magnetic semiconductor [60], and thiophene-sulfur-doped GR/ZnO nanoplate [150]. The doped ZnO or GR effectively extended its band width of light absorption into the visible region or promoted the separation of the photoinduced carriers, resulting in a significantly enhanced photocurrent response.

3.2.2. Toxins

Toxins, such as familiar microcystin-LR (MC-LR), ochratoxin A (OTA) and aflatoxin B1 (AFB₁), are poisonous substances produced within living cells or organisms. MC-LR is the most common and toxic congener in various microcystins (MCs) [165], and a type of stable heptapeptides released from cyanobacteria in diverse water environment. MC-LR is considered as a potential hepatotoxin, neurotoxin, and possibly a tumour promoter. Therefore, a maximum permitted level of 1 µg L⁻¹ was set by the WHO for MC-LR in drinking water. In addition, OTA and AFB₁ are known as powerful mycotoxins produced in improperly stored food commodities [166]. They are the most toxic and carcinogenic substances and can probably cause many types of tumour diseases in humans.

Using vertically aligned TiO₂ NTAs modified with MIP of polypyrrole (PPy), Chen et al. developed a facile PEC sensor for MC-LR determination [167]. PPy not only acted as the recognition element for MC-LR, but also efficiently promoted the separation of e–h pairs due to its π bond delocalised electron system, resulting in a higher photoelectric conversion efficiency (~16.7% of MIP@TiO₂ NTAs) than that of TiO₂ NTAs (~5.22%). With a high PEC catalytic oxidation ability towards MC-LR on the heterojunction, the designed sensor was capable of sensitively determining MC-LR with a LOD of 0.1 µg L⁻¹. As an extension of this work, Liu et al. prepared an MIP modified 1D S–C heterojunction of TiO₂ NPs/MWCNTs to detect MC-LR in real water samples [69]. The introduction of MWCNTs increased photoinduced charge transfer ability and favoured separation of e–h pairs, generating a noticeable enhanced oxidation capacity towards MC-LR. As a result, a low LOD of 0.4 pM was

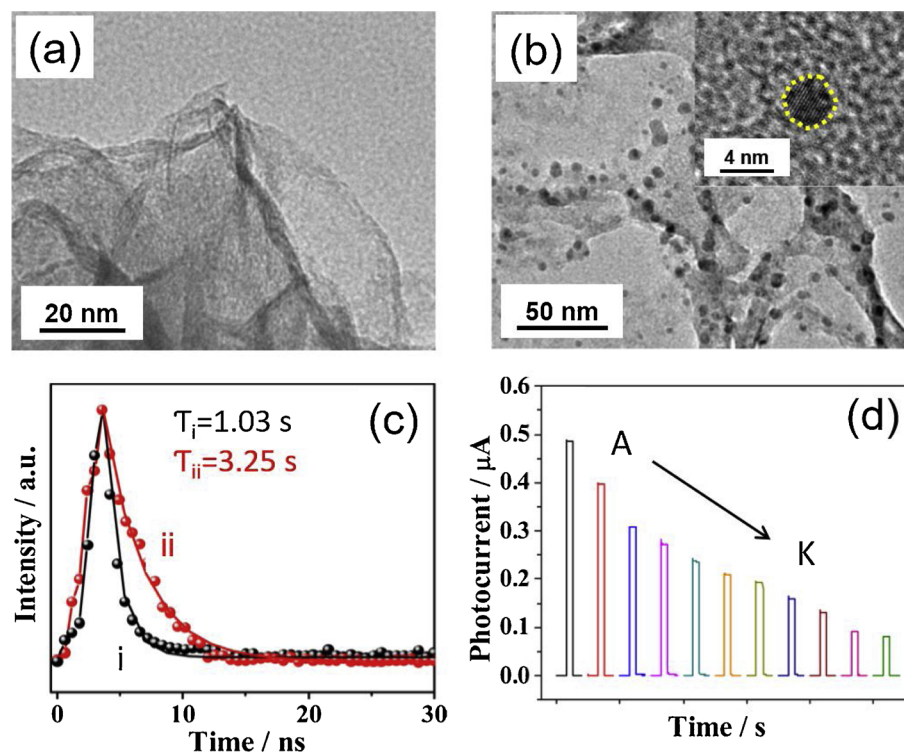


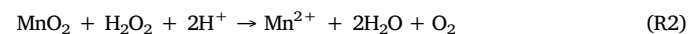
Fig. 8. (a) TEM image of ultrathin MoS₂ NSs. (b) TEM and HRTEM (inset) images of N-GR QDs/MoS₂. (c) Time-resolved transient PL decay for MoS₂ (curve i) and N-GR QDs/MoS₂ (curve ii). (d) Photocurrent responses versus the acetamiprid concentrations (from A to K: 0, 0.05, 0.1, 0.5, 1, 5, 10, 50, 100, 500 and 1000 pM). [164].

observed with this sensor. Moreover, it was applied for the accurate determination of MC-LR in real water samples with satisfactory recoveries from 96.4 to 113.0%. Other than familiar 2D GR based S-C heterojunctions, this work demonstrated the feasibility and superiority of 1D S-C heterojunctions utilising CNTs as the supporting scaffolds. For such MIP-based PEC MC-LR sensors, prominent selectivity towards a wide range of organic pollutants (e.g. atrazine, paraquat and monosulfotap) was acquired. Nevertheless, it is still a great challenge for these sensors to selectively distinguish different MCs variants, due to their highly similar molecular structures, sizes and properties.

Serving as the sacrificial agent to scavenge photoexcited holes of BiOBr NFs, the captured MC-LR molecules with aptamers facilitated the separation of the photoinduced e-h pairs [168]. With residual electrons quickly transferred to the electrode via the N-GR, an efficient MC-LR detection (LOD, 0.03 pM) was realised with the BiOBr NFs/N-GR heterojunction. In another study, a Z-scheme type CdTe QDs/Bi₂S₃ NRs heterojunction with a higher PEC activity (13 times of CdTe QDs and 2 times of Bi₂S₃ NRs) was proposed for PEC aptasensing of MC-LR [169]. With the wavelengths varying from 430 to 630 nm, a maximum photocurrent was found at 470 nm, indicating the superior visible-light driven PEC response of the heterojunction. As the binding of MC-LR on the heterointerface suppressed the electron transfer and reduced the photocurrent response, the PEC aptasensor realised an ultrasensitive determination of MC-LR (LOD, 5.0 fM). To demonstrate its practical applicability, the as-prepared aptasensor was successfully applied for trace MC-LR monitoring in tap and river water samples with acceptable recoveries (95%–110%). More importantly, in addition to common pesticide molecules, the PEC aptasensor can selectively distinguish MCs variants (e.g. MC-LA and MC-YR), effectively addressing the specificity issue on the MIP-based sensors.

Apart from the aforementioned specific assays employing MIP and aptamer as recognition elements, immunoassay provides an alternative avenue to realise a satisfactory selectivity for PEC sensing, on account of the specific discrimination reaction between the antibody and antigen [170,171]. To date, diverse heterojunctions of CdTe/Ag₂Te QDs (AFB₁) [172], CdSe NPs/TiO₂ NPs(OTA) [173], CdS NPs/rGO (MC-LR) [174], CdS NPs/B-TiO₂ NRAs and CdS NPs/TiO₂ NRAs (MC-LR) [175,176], and TiO₂

NPs/S-BiVO₄@Ag₂S NPs (OTA) [177] have been employed in PEC immunoassays of various toxins. For example, Tian et al. reported a PEC immunoassay for the determination of MC-LR in water based on a novel heterojunction of GR QDs/Si NWAs [178]. Semiconductive Si NWAs with intrinsic advantages of low toxicity, high surface area and excellent biocompatibility have attractive great interests in PEC applications [179,180]. In addition to possessing intrinsic properties of both C-QDs and GR, GR QDs was demonstrated to be sufficient barriers to prevent Si oxidation in this work. Since the specific binding of MC-LR created a barrier for the electron transfer, the resulting photocurrents decreased linearly in the concentrations from 0.1 to 10 $\mu\text{g L}^{-1}$ (LOD, 0.055 $\mu\text{g L}^{-1}$) for MC-LR. Treating with an easy regeneration process, the as-renewed sensor maintained 90.5% of the initial photocurrent value after three tests, showing an excellent reusability. Moreover, a recent work of Lin et al. performed a PEC immunoassay of AFB₁ based on a novel heterojunction of C-QDs/MnO₂ NSs [181]. Ultrathin 2D MnO₂ NSs with hypotoxicity displayed a typical sheet-like morphology and a high-degree of transparency (Fig. 9a), providing a large surface coverage for the homogeneous immobilisation of C-QDs with an average diameter from 3 to 5 nm (Fig. 9b). Serving as a typical catalytic product of glucose oxidase, the produced H₂O₂ associated with AFB₁ concentration etched the MnO₂ NSs (Reaction 2) and decomposed the heterojunction, leading to a decrease in the photocurrent (Fig. 9c). As a consequence, the PEC sensor exhibited AFB₁ within a dynamic working range from 0.01 to 20 ng mL⁻¹ with a LOD of 2.1 pg mL⁻¹ (Fig. 9d). Especially, the concentration of AFB₁ could be distinguished with the naked eye, due to the colour change of the sensing film at an increased AFB₁ level (inset in Fig. 9d). With regard to the selectivity, this sensor showed the satisfactory specificity against other mycotoxins or marine toxins, except for the AFB₂ with a similar molecular structure. Stimulated by the enormous demands for environmentally friendly photoactive nanomaterials in practical applications, these innovative researches exhibit promising paradigms for designing desirable heterojunctions with low toxicity, high photostability and excellent PEC activity.



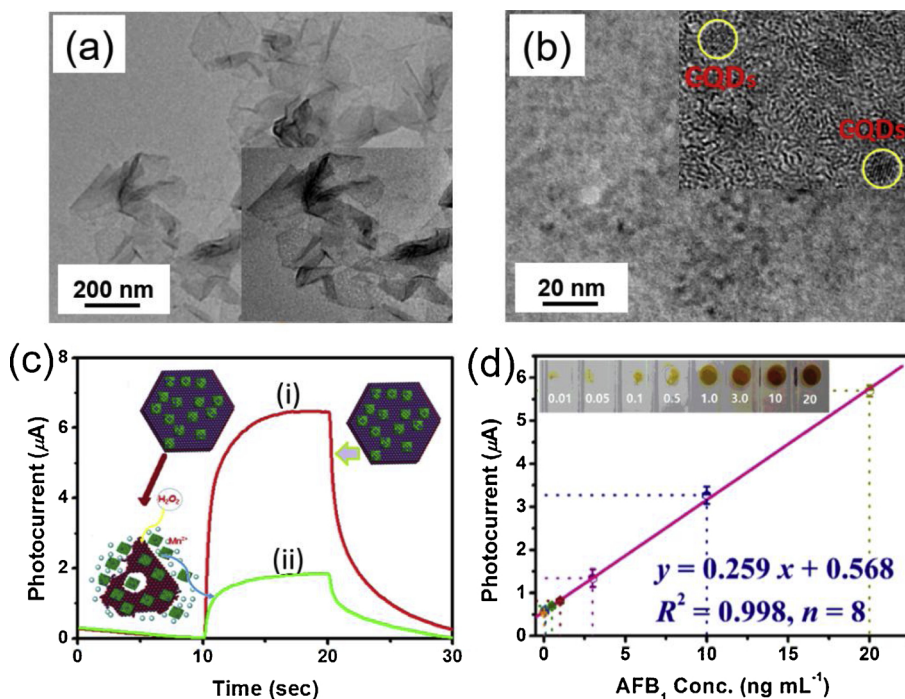


Fig. 9. TEM images of (a) MnO₂ NSs and (b) C-QDs/MnO₂ NSs. Insets: the corresponding magnification images. (c) Photocurrent responses of C-QDs/MnO₂ NSs in the (i) absence and (ii) presence of H₂O₂. (d) Linear calibration curve of photocurrents versus AFB₁ concentrations. Inset: the corresponding photograph of C-QDs/MnO₂ NSs after the measurement [181].

Table 3
Photoactive nanomaterials based PEC monitoring of phenolics in environmental samples.

Photoactive nanomaterial	Recognition element	Target	Linear range	LOD	Real sample	Ref.
Porphyrin/Au NPs/GR	N/A	Hydroquinone (HQ)	20-240 nM	4.6 nM	N/A	[188]
Bi ₂ WO ₆ /N-GR QDs		Pentachlorophenol (PCP)	0.2 pM-1 nM	0.06 pM	River water	[189]
α-Fe ₂ O ₃ NPs/N-GR		HQ	3.0 nM-3.3 μM	1.0 nM	Waste water	[190]
Cu ₂ O NPs/rGO		HQ	5.0 μM-1.0 mM	0.5 μM	N/A	[191]
g-CN/BiOI		BPA	80-3200 ng mL ⁻¹	26 ng mL ⁻¹	River water	[192]
Au NPs/g-C ₃ N ₄		4-chlorophenol	0.25-34.70 μM	0.08 μM	River water	[193]
NiO/Co ₃ O ₄ /g-C ₃ N ₄		TBBPA ^a	0.3-500 μM	0.1 μM	River/lake water	[194]
Au NPs/BiOCl		4-chlorophenol	0.16-20 mg L ⁻¹	0.05 mg L ⁻¹	N/A	[195]
[Ru(bpy) ₃] ²⁺ /SnO ₂ NPs ^b	MIP	BPA	2-500 nM	1.2 nM	Tap/River water	[196]
TiO ₂ NTAs		BPA	4.5-108 nM	2.0 nM	Domestic sewage	[197]
CdS QDs/GR		4-aminophenol	50 nM-3.5 μM	23 nM	Lake water	[198]
CdSe _{0.75} Te _{0.25} /TiO ₂ NTAs	Antibody	PCP	1 nM-0.3 μM	1 pM	River water	[199]
CdSe QDs/TiO ₂	Aptamer/DNA	2-aminophenol	0.4-27 μM	80 nM	N/A	[200]
TiO ₂ NPs/N-GR		BPA	1 fM-10 nM	0.3 fM	Mineralised water	[201]
CdS QDs/GR		Catechol	10 nM-1.0 μM	4.9 nM	Lake water	[202]

^a TBBPA: tetrabromobisphenol A; ^b[Ru(bpy)₃]²⁺: tris(2,2'-bipyridine)ruthenium(2+).

3.2.3. Phenolics

As typical polar compounds, phenolics usually have a high tendency to stay in aquatic media. Once being introduced into the ecosystem, they would adversely affect the indigenous biota, such as reduced fertility, decreased survival of the young, and inhibition of growth. For example, bisphenol A (BPA) is known as one of the environmental endocrine disrupting chemicals, which can mimic the function of hormone oestradiol, bind to and activate the oestrogen receptor and disrupt the endocrine system of human beings [182]. Exposure to BPA is considered to be associated with many adverse effects including cardiovascular diseases, obesity, carcinogenicity, neurotoxicity and developmental problems. Therefore, great efforts have been dedicated to developing versatile PEC sensors for the determination of phenolics, as summarised in Table 3.

Through quickly annealing TiO₂ NTAs in the presence of residual ethylene glycol and the subsequent electrodeposition of Au NPs, a robust 3D heterojunction of Au NPs/C-TiO₂ NTAs was prepared for the PEC sensing of BPA [183]. Due to the capillary effect of the NTs, Au NPs (4-8 nm in diameter) were homogeneously deposited in both inside/outside the NT walls, sufficiently utilising the available surface of NTs

and achieving an excellent PEC catalytic activity. As a result, the PEC sensor showed a LOD of 6.2 nM for BPA detection, as well as a good specificity towards some phenolic derivatives (e.g. phenol, 4-nitrophenol, 3,5-dimethylphenol, and 4-fluorophenol). Interestingly, dealing with the UV irradiation, this robust heterojunction could be readily renewed without damaging the microstructures and surface states, and a subtle change (RSD of 3.0%) in sensitivity was observed after five fouling/refreshing runs.

Via forming a five/six-atom ring structure between Ti⁴⁺ sites and adjacent double oxygen atoms in the o-diphenol, an attractive S-S heterojunction of WS₂/TiO₂ was designed for the detection of o-diphenol and its derivatives [184]. As a member of transition-metal dichalcogenide, layered WS₂ exhibited excellent physical, electronic and optical prosperities, and the matched band levels with TiO₂ made photogenerated e-h pairs easily separated. In view of the favourable chelate effect, such a biomolecule-free PEC sensor demonstrated low detection limit (e.g. 0.32 μM for dopamine) and excellent stability, as well as cost-effective advantages.

Recently, a variety of recognition elements (aptamer, antibody and MIP) have been screened and employed to realise excellent selective PEC

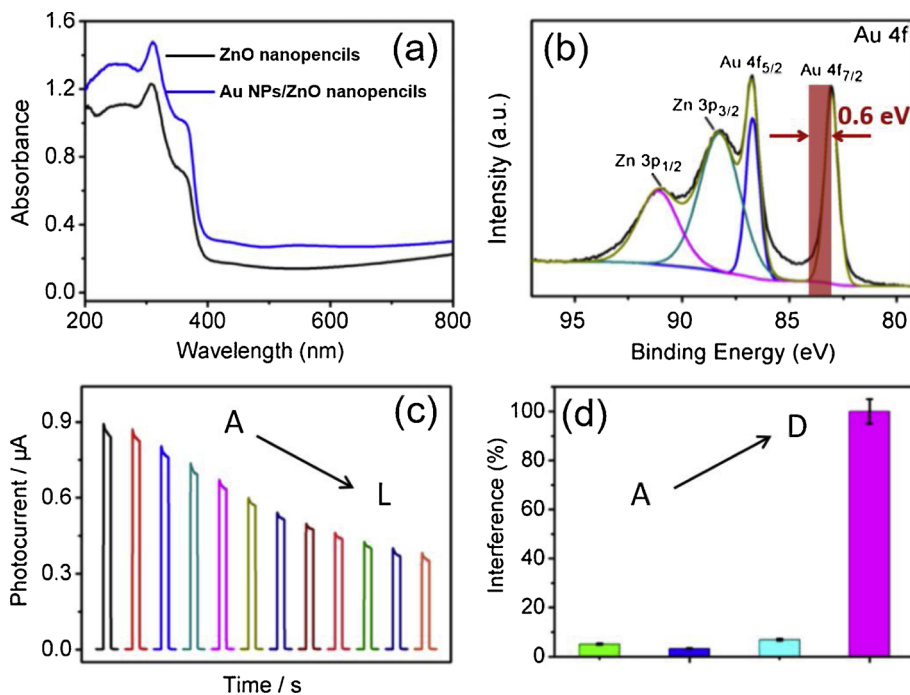


Fig. 10. (a) UV-vis diffuse reflection of ZnO nanowires and Au NPs/ZnO nanowires. (b) High-resolution XPS spectrum of Au_{4f}. (c) Photocurrents versus different BPA concentrations (from A to L: 0, 1, 5, 10, 30, 60, 100, 200, 400, 600, 800 and 1000 nM). (d) Selectivity of the PEC aptasensor for BPA detection (from A to D: 4,4'-bisphenol, 6 F bisphenol A, bisphenol B and BPA). [185].

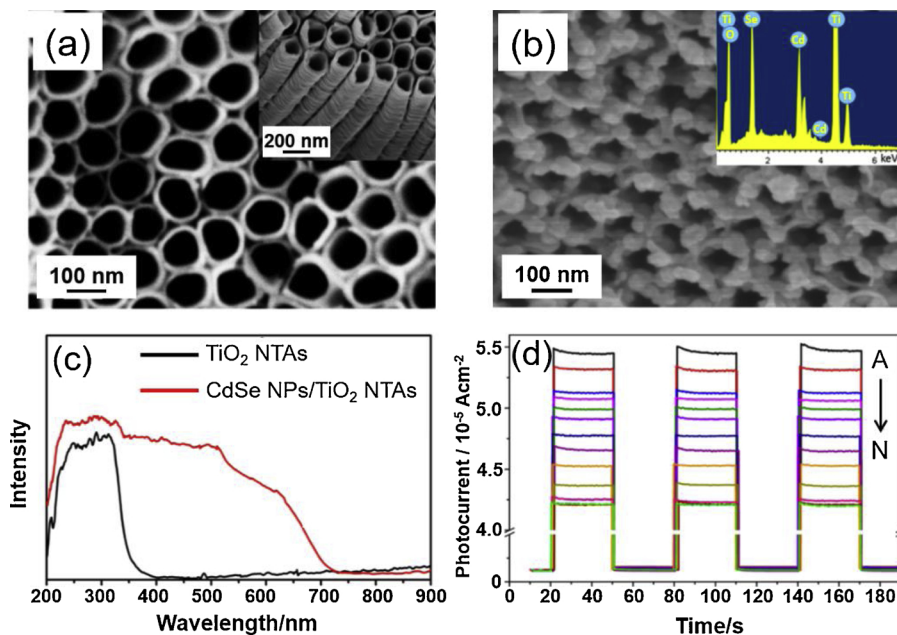
analysis for phenolics. For instance, Qiao et al. reported a sensitive PEC aptasensor for BPA detection based on a S–M heterojunction of Au NPs/ZnO nanowires [185]. Attributed to the SPR effect of Au NPs, remarkably enhanced absorption in the visible wavelength of 500–800 nm was observed on the heterojunction (Fig. 10a). The binding energy at 83.4 eV of Au_{4f}_{7/2} with a negative shift (~0.6 eV) in comparison to bulk Au revealed a facilitated interfacial electron transfer (Fig. 10b), primarily ascribed to the strong electronic interaction between Au NPs and ZnO. Since the presence of BPA blocked the photogenerated electron-transfer channels, the assembled PEC aptasensor was linear with the concentration of BPA in the range of 1–1000 nM with a LOD of 0.5 nM (Fig. 10c). Considering a high specificity between the aptamer and BPA, a satisfactory selectivity towards other familiar interferences was achieved (Fig. 10d). Similarly, Wang et al. reported a PEC immunosensor for tetrabromobisphenol A (TBBPA) based on 2D Au NPs/MoS₂ NSs [186]. It was demonstrated that Au NPs immobilised in a close proximity to each other on MoS₂ NSs (via Au-S bond) was critical to enhance the SPR effect and acquired a sensitive photocurrent response. Accordingly, the fabricated PEC sensor showed a sensitive detection for TBBPA with a wide linear range from 0.1 nM to 1.0 μM (LOD, 45 pM) and high storage stability (93.3%, 2 weeks). Moreover, as an extension to their previous work involving microfluidic paper-based analytical device, Sun et al. established a visible light PEC sensing platform for pentachlorophenol (PCP) based on PPy/ZnO NPs decorated Au-PWE [187]. With adsorbed PCP increased the steric hindrance for electron transfer, the PEC analytical device realised a sensitive detection of PCP with a LOD of 4 pg mL⁻¹. Coupling with appropriate photoactive materials, it is highly anticipated that the disposable microfluidic device would have wide applications in the PEC monitoring.

3.2.4. Antibiotics

As typical members of broad-spectrum antibiotics, tetracycline (Tc) and chloramphenicol (CAP) are extensively used for agricultural purposes and human therapy. However, the abuse of these antibiotics causes the accumulation of the antibiotics in animal products. Even after being discharged into the environment, they are difficult to be degraded in the short term, resulting in lasting environmental problems including ecological risks and human health damage [203]. Therefore, developing sensitive and specific approaches are highly desirable for the detection of these antibiotics.

A recent work by Yan et al. showed a facile PEC sensor for monitoring Tc based on a flower-like S–S heterojunction of carbon nitride (CN)/BiOBr [204]. Prepared via one-pot ST process with the addition of ionic liquid [C₁₆mim]Br, the unique flower-like structure assembled with numerous BiOBr NSs (~20 nm in thickness) afforded a large area for anchoring thin CN NSs. The presence of ionic liquid improved the dispersity of CN on the surface of BiOBr, resulting in the formation of a high-quality heterojunction. Due to a drastically improved PEC ability (6 times of BiOBr) towards the selective oxidation of Tc, the prepared PEC sensor exhibited a LOD of 3.8 ng mL⁻¹ with two linear relationships (8.0–400 ng mL⁻¹ and 400–5200 ng mL⁻¹), excellent storage stability (95.8%, 3 weeks), and good anti-interference ability for Tc detection.

Furthermore, to improve the assay selectivity, a visible-light PEC aptasensor for Tc determination was constructed on 2D CdS QDs/g-C₃N₄ [205]. Layered g-C₃N₄ has been widely used for the effective loading and dispersion of QDs, achieving the construction of various high-performance heterojunctions [206,207]. In this work, CdS QDs (~4 nm in diameter) were homogeneously and densely dispersed on g-C₃N₄ with closely contacted interfaces. With captured Tc molecules participating in the PEC oxidation process, an increased linear response of the PEC sensor from 10 to 250 nM with a LOD of 5.3 nM was observed. The proposed PEC sensor was successfully applied to Tc detection in water samples with high precision and accuracy (recoveries from 98.2% to 101.1%). With the same sensing strategy, Liu et al. constructed a facile PEC aptasensor for CAP detection, utilising N-GR QDs as the transducer species [208]. Synthesised via a facile one-step HT method, N-GR QDs prepared in this work exhibited a high optoelectronic conversion efficiency (2 times of GR QDs) under visible light irradiations ($\lambda > 420$ nm), demonstrating that nitrogen doping obviously enhanced the absorption and electron transfer ability. Therefore, this sensor showed a linear PEC response to CAP concentration in the range of 10–250 nM (LOD, 3.1 nM) with satisfactory selectivity and storage stability. Moreover, utilising the SPR effect on the Au NPs/TiO₂ NPs heterojunction, Li et al. built another PEC aptasensor for Tc detection [209], in which quercetin was chosen as both a photosensitiser and electron donor for signal amplification. Since the formation of Tc-aptamer complex blocked the long passage ways of electron transfer, gradually decreased photocurrents ranging from 0.3 to 1600 nM were observed for Tc assay (LOD, 0.1 nM).



3.2.5. Hormones

Steroid hormones, such as 17 β -estradiol (E2), have attracted great attention in environmental and biomedical fields due to their harmful effects on the endocrine function of human and animals [210]. The presence of low concentration of hormone in the environment can cause the abnormal sexual development of animals and decrease the average number of human spermatozoa.

Fan et al. developed a sensitive PEC aptasensor for E2 detection using the vertically aligned 3D CdSe NPs/TiO₂ NTAs prepared by anodisation and electrodeposition methods [211]. Vertically oriented TiO₂ NTAs (50–100 nm in diameter) were successfully fabricated with a wall thickness of ~10 nm and length of ~1 μ m (Fig. 11a). The hollow tube architecture not only provided an accessible area for depositing CdSe NPs, but promoted the directional charge transport ability. As a consequence, CdSe NPs with an average diameter of ~30 nm were uniformly dispersed on the TiO₂ NTAs, offering multidimensional spaces for immobilising aptamer molecules (Fig. 11b). Thanks to the obvious absorption extending to ~730 nm on the heterojunction, it was not only critical to enhance visible-light absorption, but also avoid the damage of aptamer bioactivity under the UV irradiation (Fig. 11c). Particularly, a robust photocurrent response was achieved after 30 times irradiation due to its splendid stability of the heterojunction. With the formation of E2-aptamer complexes retarded the movement of electron donor, gradually decreased photocurrents in a range from 0.05 to 15 pM were observed (Fig. 11d). The LOD for E2 was calculated to be 33 fM, and the selective sensor was successfully applied in the detection of E2 in medical wastewater, tap and lake waters. With a similar strategy, Liu et al. constructed another visible-light driven PEC aptasensor for E2 detection, based on a novel S-S heterojunction of BiVO₄ NPs/TiO₂ nanospheres [212]. The intimate interface facilitated the electron transfer within the heterojunction and improved the separation of photo-generated charges. The proposed PEC sensor showed a low LOD of 22 fM for E2, and excellent selectivity towards common coexisted species (e.g. estriol, 1-aminoanthraquinone, ethinylestradiol, testosterone and BPA).

Making use of the SPR effect of Au NRs on α -Fe₂O₃/N-GR, Du et al. developed a highly sensitive PEC aptasensor for trace E2 assay [213]. 2D N-GR with a high surface area provided numerous nucleation and binding sites for anchoring well-dispersed α -Fe₂O₃ nanocrystals and Au NRs. Owing to the suitable spectral overlap between the plasmonic Au NRs and α -Fe₂O₃ [214], an obvious enhancement in the spectral response would be observed on the heterointerface. With the dissociation

Fig. 11. (a) Top and cross-sectional (inset) SEM images of TiO₂ NTAs. (b) SEM image and EDS spectrum (inset) of CdSe NPs/TiO₂ NTAs. (c) UV-vis spectra of TiO₂ NTAs and CdSe NPs/TiO₂ NTAs. (d) The photocurrents versus different concentrations of E2 (A to N: 0, 0.05, 0.07, 0.09, 0.15, 0.3, 0.6, 2.4, 4.8, 9.6, 15, 35, 50, 80 pM, respectively) [211].

of E2/aptamer complexes on the heterointerface reduced steric hindrance, the as-prepared PEC aptasensor exhibited superb analytical performances for E2 detection, e.g. an ultralow LOD of 0.33 fM, high specificity and excellent stability with no obvious change in photocurrents for 2 weeks.

Possessing a high adsorption capacity towards a variety of Cd²⁺, Zn²⁺ and Ag⁺ ions [215,216], titanium phosphate (TiP) NPs is considered as a fascinating scaffold for anchoring desirable photoactive materials, such as CdS, ZnS and AgI, opening a new avenue for preparing heterojunctions with high PEC activities. As an attempt, Li et al. proposed a PEC immunoassay protocol for E2 detection based on the CdS NPs/TiP NPs/TiO₂ film [217]. Porous TiP NPs (~55 nm in diameter) provided numerous sites for Cd²⁺ sorption, followed by the in-situ generation of CdS NPs through S²⁻ deposition on TiO₂ film. Hence, the obtained heterojunction exhibited highly stable and remarkably enhanced photocurrents during on/off irradiation cycles for 300 s. The exploration of the relationship between wavelengths (365–570 nm) and photocurrents revealed an optimal photocurrent response at ~430 nm, confirming that the photocurrent originated mainly from the excitation of the in-situ generated CdS NPs. Via a competitive binding protocol, the proposed biosensor showed a LOD down to 2 pg mL⁻¹ for E2 detection with high selectivity, and demonstrated a successful assay in the lake water with recoveries between 104.7 and 108.1%.

3.2.6. Others

Polychlorinated biphenyls (PCBs), known as persistent organic pollutants, exhibit diverse toxic effects such as carcinogenicity and endocrine disruption. Shi et al. reported highly selective and sensitive PEC sensors for the rapid detection of PCB 101 in environmental water samples, employing MIP modified 3D TiO₂ NRAs and Pd QDs/TiO₂ NRAs [67,218]. Pd QDs with an appropriate size of ~4.0 nm were uniformly decorated on TiO₂ NRAs, forming an intact hetero-interface to achieve an excellent PEC catalytic activity. The positive shift in the Mott-Schottky plots of the potential of flat band (E_{FB} , from -0.271 V to -0.085 V) after Pd QDs modification demonstrated a decreased bending of the band edge, realising a beneficial electron transfer for the Pd QDs/TiO₂ NRAs. With an excellent PEC reduction activity towards PCB 101, an improved PEC sensing with a LOD of 50 fM was obtained, giving a linear range from 0.1 pM to 0.5 nM. The PEC sensor was then successfully applied for PCB 101 detection in real water and soil samples [67]. Except for the congeners of PCB 126 and PCB 77 with similar chemical structure and molecular shape, the sensor exhibited acceptable assay

specificity.

Acting as photogenerated hole scavengers, organic pollutants of p-phenylenediamine (PPD) and 4-methylimidozal (4-MID) have also been successfully determined with the PEC methods [219,220]. For instance, Dai et al. developed a novel heterojunction of TiO₂ mesocrystal/Poly(l-cysteine) (PLC)/carbon nanohorns (CNHs) for the PEC detection of 4-MID [220]. Porous TiO₂ superstructures possessed a very large specific surface area (~211 m² g⁻¹), high-reactive (001) facets and superior photocatalytic activity, achieving a significantly enhanced photoelectric conversion efficiency (~1.76 times of P25). Assembled with many single-layer GR sheets, hierarchical CNHs were served as an excellent electron-transport scaffold for anchoring TiO₂ mesocrystal, using PLC as a link-agent. As expected, the fabricated sensor showed a wide linear range from 0.1 nM to 0.1 mM (LOD, 30 pM), with a good reproducibility (RSD of 3.58%, n = 3) and storage stability. Towards selected interfering substances, such as glucose, trisodium citrate and arginine, a high selectivity of the present sensor for 4-MID detection was demonstrated.

As an extension to their previous work, Gong et al. designed MIP modified AgI NPs/BiOI NFAs for a signal-off PEC detection of perfluorooctanoic acid (PFOA) [221]. Uniform AgI NPs (~30 nm in diameter) were homogeneously anchored in a 3D framework of interlaced BiOI NFAs, providing an ideal matrix for grafting of MIP and exhibiting a substantial improvement in photocurrent. Due to the increased steric hindrance produced in the presence PFOA, such a PEC sensor was successfully used for PFOA detection (LOD, 0.01 ppb) with satisfactory specificity and storage stability (92%, 30 days).

With a similar sensing strategy, an ideal stepwise band-edge MC heterojunction of CdTe QDs/CdS QDs/TiO₂ NTAs was developed for a PEC immunosensor towards the detection of octachlorostyrene (OCS) [222]. The hollow NTAs not only provided a high accessible area for the deposition of QDs, but also served as an excellent collector to capture electron flow from CdTe and CdS due to the Fermi level difference. With the binding of OCS obstructed the transport of reduced reagent to the heterojunction surface, the PEC immunosensor displayed a linear range from 5 pM to 50 nM (LOD, 2.58 pM) towards OCS determination, a high specificity and storage stability (95%, 4 months).

3.2.7. Perspectives

In the past few years, significant advancements have been achieved in the development of competent heterojunctions for the PEC monitoring of various organic pollutants. With a tailored structure, composition and morphology, versatile heterojunctions effectively overcome many drawbacks of a pristine photoactive material. Particular attention has been paid to fascinating heterojunctions with the preferred morphologies of 2D NSs, and 3D NRAs and NTAs, mainly ascribed to their large specific surface area, fast electrical transfer, homogeneous hetero-interfaces, and a superior optoelectronic response.

However, several critical issues still remained to be resolved before these promising PEC sensors can be put into practical applications. According to the literatures, a large part of reported PEC sensors was performed using the target as the electron donor. Despite its simplicity, more explorations and improvements should be implemented to address the potential interference existing in a complex real sample. Therefore, developing novel photoactive materials with intrinsically special interaction towards organic analytes (e.g. the chelation or coordination) is highly anticipated in future research. Meanwhile, due to the possible adsorption of organic molecules and their derivations on the surface of heterojunctions, the fouling issue should be taken into consideration, which will definitely reduce the light absorption and disturb the assay precision and repeatability. Moreover, theoretical calculations (e.g. density functional theory simulations) for understanding and optimising the charge-separation mechanism at the interfaces can be referred for rapid and systematic screening of desired photoactive materials. This would in turn make the experimental exploration of novel heterojunctions more efficient and worthwhile.

Finally, cost-effective and reliable PEC determination would definitely have a great potential in practical applications. In this regards, developing promising synthesis procedures for the preparation of highly stable photoactive materials is desirable in future work. On one hand, facile and reliable procedures can not only reduce the production cost, but improve the assay reproducibility. On the other hand, photoactive materials with a highly stability are favourable for the long term storage and usage.

3.3. PEC monitoring of other inorganic pollutants

In addition to metal ions and organic pollutants, other toxic inorganic pollutants of cyanide, nitrate, hydrazine and sulfide have received much attention due to their severe environmental hazards [223,224]. For instance, the long-term ingestion and accumulation of high levels of nitrite or sulfide into the human body will lead to losing consciousness and discomfort in the mucous membranes, and even permanent brain damage.

Through designing a new MC heterojunction of TiO₂ NWs/GR/polymer nanosponge (PNS) prepared by assembling 1D TiO₂ NWs and 2D GR into 3D PNS, Muthuchamy et al. constructed an efficient PEC biosensing platform for the nitrite determination (LOD, 0.225 μM) [225]. 3D conductive PNS consisting of interconnected porous network structures was demonstrated to be an efficient matrix for loading photoactive materials and biological enzyme. With a comparable property of PNS, 3D porous graphene structures are extremely anticipated in the construction of superior heterojunctions, due to their large specific area, favourable diffusion profile and fast electron transfer rate [226,227]. Particularly, these in-situ generated 3D graphene films possessed significantly enhanced binding strengths on the substrates and controllable morphologies, opening a new horizon for the development of high-performance PEC sensors. Moreover, utilising the high and robust PEC catalytic ability towards hydrazine, sensitive PEC sensors for the determination of hydrazine were acquired on TiO₂ NWAs and TiO₂ NPs respectively, achieving the precise detection at micromolar level in water samples [228,229].

Lately, Su et al. described a PEC sensing of sulfide based on a S-S heterojunction of Cu₂O NPs/TiO₂ NTAs, prepared with the electrochemical anodisation and deposition method [230]. Similar with the replacement strategy used for PEC Cu²⁺ detection, an e-h pair recombination centre of Cu₇S₄ was formed on the heterojunction surface in the presence of sulfide, leading to a selective decrease in the photocurrent response with visible light irradiation ($\lambda > 400$ nm). The PEC sensor exhibited a LOD of 0.6 μM over a linear response range from 1 to 300 μM, high selectivity (< 5% responses towards 10-fold SiO₃²⁻, HPO₄²⁻, SO₃²⁻, CO₃²⁻, Br⁻ and Cl⁻) and satisfactory recoveries (99.2–102.9%) for tap and lake water samples.

4. Conclusions

This review introduces the recent research progress on engineered photoactive nanomaterials, and their elegant applications in the PEC monitoring of toxic environment pollutants. The advantages of PEC sensors, e.g. high sensitivity, fast response, low cost and especially easy miniaturisation, have been well acknowledged. The progress in this field indicates that doping or forming heterojunction affords an effective and promising route to boost the PEC activity of a single semiconductor.

In the view of material design and fabrication, particular attention should be focused on two of the main aspects for the development of high-performance PEC sensors in the future. One important point is to develop novel photoactive heterojunctions with excellent PEC properties. Preferred materials for engineering a heterojunction should generally meet the following requirements, (i) excellent visible-light response, (ii) fast transfer capacity for charge carriers, (iii) high optoelectronic conversion efficiency, (iv) congruent bandgap structure

for redox reactions, and (v) robust photostability for long-term applications. MC heterojunctions usually possess high PEC activity and sensitivity. Nevertheless, it should be noted that the complicated synthesis procedures require more exquisite operations, which is not favourable for obtaining a reliable assay with satisfactory reproducibility. Therefore, a balance between the sensitivity and reliability of PEC sensors should be taken into consideration for the practical applications. Meanwhile, realising a controllable regulation on the morphology of heterojunctions plays another critical role in improving their sensing performance. Compared with diverse 0D, 1D and 2D architectures, 3D architectures could support fast electron transfer in multidimensional space, enable rapid ion diffusion and mass transfer at the interfaces, and provide adequate effective area for the recognition and testing process. In addition to common 3D array architectures, 3D porous graphene-based heterojunctions are also extraordinarily anticipated for achieving excellent PEC performances, owing to their tunable porous scaffolds, excellent compatibility with most inorganic nanostuctures, and superior mechanical flexibility.

Despite the rapid progress in this field, some fundamental issues and technological challenges must be addressed to fully realise the practical applications of constructed PEC sensors. Although possessing adjustable band gaps and size, the inherent toxicity of most traditional QDs (e.g. CdS and CdSe) would lead to the secondary pollution in the usage. Therefore, more research efforts should be invested to develop environmental-friendly photoactive species, e.g. C-QDs and GR QDs. In addition, although multiple strategies have been proposed for the preparation of various heterojunctions, it is still challenging to develop facile and efficient methods for the production of high-quality heterojunctions at a large scale. Moreover, precise control over the morphology including the size, distribution and contact interface is highly desirable to ensure a satisfactory stability and reproducibility of the PEC test. Further progress in these aspects of heterojunctions is possible in conjunction with the sustainable development of nanoscience and nanotechnology. In addition, most of the PEC sensors reported so far in the literatures have been tested in laboratory research. For the field monitoring of environmental samples, it is highly desired to combine the PEC technique with paper working electrode based microfluidic systems for rapid, simultaneous and multichannel detection. This advancement will facilitate the miniaturisation design and assist their integration into portable and smart devices. All the above aspects are essential for establishing a sustainable development of PEC sensing platform from fundamental research to commercial applications.

Acknowledgements

The author (Sun) would like to express his thanks to the support from Vice-Chancellor's Professorial Research Fellowship, Edith Cowan University.

References

- [1] C.H. Wu, C. Maurer, Y. Wang, S.Z. Xue, D.L. Davis, Environ. Health Perspect. 107 (1999) 251–256.
- [2] Z.Y. Li, Z.W. Ma, T.J. van der Kuij, Z.W. Yuan, L. Huang, Sci. Total Environ. 468 (2014) 843–853.
- [3] F.P. Perera, V. Rauh, W.Y. Tsai, P. Kinney, D. Camann, D. Barr, T. Bernert, R. Garfinkel, Y.H. Tu, D. Diaz, J. Dietrich, R.M. Whyatt, Environ. Health Perspect. 111 (2003) 201–205.
- [4] R.P. Schwarzenbach, T. Egli, T.B. Hofstetter, U. von Gunten, B. Wehrli, Annu. Rev. Environ. Resour. 35 (2010) 109–136.
- [5] W.W. Zhao, J.J. Xu, H.Y. Chen, Chem. Soc. Rev. 44 (2015) 729–741.
- [6] Y. Zang, J.P. Lei, H.X. Ju, Biosens. Bioelectron. 96 (2017) 8–16.
- [7] R. Freeman, J. Girsh, I. Willner, ACS Appl. Mater. Interfaces 5 (2013) 2815–2834.
- [8] W.W. Zhao, J.J. Xu, H.Y. Chen, Chem. Rev. 114 (2014) 7421–7441.
- [9] W.G. Ma, D.X. Han, M. Zhou, H. Sun, L.N. Wang, X.D. Dong, L. Niu, Chem. Sci. 5 (2014) 3946–3951.
- [10] Y. Cai, R. Kozhummal, C. Kubel, V. Trouillet, M. Bruns, S. Gutsch, M. Zacharias, Y. Yang, J. Mater. Chem. A Mater. Energy Sustain. 5 (2017) 14397–14405.
- [11] H. Wang, H.L. Ye, B.H. Zhang, F.Q. Zhao, B.Z. Zeng, J. Mater. Chem. A Mater. Energy Sustain. 5 (2017) 10599–10608.
- [12] J. Qian, Z. Yang, C. Wang, K. Wang, Q. Liu, D. Jiang, Y. Yan, K. Wang, J. Mater. Chem. A Mater. Energy Sustain. 3 (2015) 13671–13678.
- [13] S.S. Liu, S.L. Zhao, W.W. Tu, X.Y. Wang, X. Wang, J.C. Bao, Y. Wang, M. Han, Z.H. Dai, Chem. Eur. J. 24 (2018) 3677–3682.
- [14] J. Shu, Z.L. Qiu, J.Y. Zhuang, M.D. Xu, D.P. Tang, ACS Appl. Mater. Interfaces 7 (2015) 23812–23818.
- [15] J.Q. Tian, H.J. Zhu, J. Chen, X.T. Zheng, H.W. Duan, K.Y. Pu, P. Chen, Small 13 (2017) 1700798.
- [16] J. Shu, D.P. Tang, Chem.-Asian. J. 12 (2017) 2780–2789.
- [17] W.W. Zhao, J.J. Xu, H.Y. Chen, Biosens. Bioelectron. 92 (2017) 294–304.
- [18] J. Tang, Y.C. Wang, J. Li, P.M. Da, J. Geng, G.F. Zheng, J. Mater. Chem. A Mater. Energy Sustain. 2 (2014) 6153–6157.
- [19] L.P. Chen, J.B. Cui, X. Sheng, T.F. Xie, T. Xu, X.J. Feng, ACS Sens. 2 (2017) 1567–1572.
- [20] R. Asahi, T. Morikawa, H. Irie, T. Ohwaki, Chem. Rev. 114 (2014) 9824–9852.
- [21] F. Wang, J.H. Seo, Z.D. Li, A.V. Kvit, Z.Q. Ma, X.D. Wang, ACS Appl. Mater. Interfaces 6 (2014) 1288–1293.
- [22] S. Ameen, M.S. Akhtar, H.K. Seo, Y.S. Kim, H.S. Shin, Chem. Eng. J. 187 (2012) 351–356.
- [23] Y. Cong, J.L. Zhang, F. Chen, M. Anpo, J. Phys. Chem. C 111 (2007) 6976–6982.
- [24] Y.C. Zhang, M. Yang, G.S. Zhang, D.D. Dionysiou, Appl. Catal. B-Environ. 142 (2013) 249–258.
- [25] D. Qu, M. Zheng, L.G. Zhang, H.F. Zhao, Z.G. Xie, X.B. Jing, R.E. Haddad, H.Y. Fan, Z.C. Sun, Sci. Rep. 4 (2014) 5294.
- [26] L. Tang, R. Ji, X. Li, G. Bai, C.P. Liu, J. Hao, J. Lin, H. Jiang, K.S. Teng, Z. Yang, S.P. Lau, ACS Nano 8 (2014) 6312–6320.
- [27] D.Y. Pan, J.C. Zhang, Z. Li, M.H. Wu, Adv. Mater. 22 (2010) 734–738.
- [28] L. Wang, L. Wang, T. Xu, H.B. Liao, C.J. Yao, Y. Liu, Z. Li, Z.W. Chen, D.Y. Pan, L.T. Sun, M.H. Wu, Nat. Commun. 5 (2014) 5357.
- [29] J. Moon, J. An, U. Sim, S.P. Cho, J.H. Kang, C. Chung, J.H. Seo, J. Lee, K.T. Nam, B.H. Hong, Adv. Mater. 26 (2014) 3501–3505.
- [30] S.J.A. Moniz, S.A. Shevlin, D.J. Martin, Z.X. Guo, J.W. Tang, Energy Environ. Sci. 8 (2015) 731–759.
- [31] A. Kongkanand, K. Tvrđić, K. Takechi, M. Kuno, P.V. Kamat, J. Am. Chem. Soc. 130 (2008) 4007–4015.
- [32] D.I. Son, B.W. Kwon, D.H. Park, W.S. Seo, Y. Yi, B. Angadi, C.L. Lee, W.K. Choi, Nat. Nanotechnol. 7 (2012) 465–471.
- [33] H.T. Li, X.D. He, Z.H. Kang, H. Huang, Y. Liu, J.L. Liu, S.Y. Lian, C.H.A. Tsang, X.B. Yang, S.T. Lee, Angew. Chem. Int. Ed. 49 (2010) 4430–4434.
- [34] V.D. Mihaileci, H.X. Xie, B. de Boer, L.J.A. Koster, P.W.M. Blom, Adv. Funct. Mater. 16 (2006) 699–708.
- [35] J. Li, W. Tu, H. Li, M. Han, Y. Lan, Z. Dai, J. Bao, Anal. Chem. 86 (2014) 1306–1312.
- [36] J.Y. Liu, H. Xu, Y.G. Xu, Y.H. Song, J.B. Lian, Y. Zhao, L. Wang, L.Y. Huang, H.Y. Ji, H.M. Li, Appl. Catal. B-Environ. 207 (2017) 429–437.
- [37] X.M. Li, M.C. Rui, J.Z. Song, Z.H. Shen, H.B. Zeng, Adv. Funct. Mater. 25 (2015) 4929–4947.
- [38] A. Mishra, P. Bauerle, Angew. Chem. Int. Ed. 51 (2012) 2020–2067.
- [39] Y. Diao, L. Shaw, Z.A. Bao, S.C.B. Mannsfeld, Energy Environ. Sci. 7 (2014) 2145–2159.
- [40] D. Chen, H. Zhang, Y. Liu, J.H. Li, Energy Environ. Sci. 6 (2013) 1362–1387.
- [41] H.Q. Sun, S.B. Wang, Energy Fuels 28 (2014) 22–36.
- [42] J.C. Liu, H.W. Bai, Y.J. Wang, Z.Y. Liu, X.W. Zhang, D.D. Sun, Adv. Funct. Mater. 20 (2010) 4175–4181.
- [43] M. Shah, A.R. Park, K. Zhang, J.H. Park, P.J. Yoo, ACS Appl. Mater. Interfaces 4 (2012) 3893–3901.
- [44] A. Kongkanand, R.M. Dominguez, P.V. Kamat, Nano Lett. 7 (2007) 676–680.
- [45] L.F. Yue, S.F. Wang, G.Q. Shan, W. Wu, L.W. Qiang, L.Y. Zhu, Appl. Catal. B-Environ. 176 (2015) 11–19.
- [46] Y.N. Zhang, N. Qin, J.Y. Li, S.N. Han, P. Li, G.H. Zhao, Appl. Catal. B-Environ. 216 (2017) 30–40.
- [47] A.K. Geim, K.S. Novoselov, Nat. Mater. 6 (2007) 183–191.
- [48] L. Shi, Y. Wang, S. Ding, Z. Chu, Y. Yin, D. Jiang, J. Luo, W. Jin, Biosens. Bioelectron. 89 (2017) 871–879.
- [49] Y. Yin, L. Shi, Z. Chu, W. Jin, RSC Adv. 7 (2017) 45053–45060.
- [50] X.R. Zhang, S.G. Li, X. Jin, S.S. Zhang, Chem. Commun. 47 (2011) 4929–4931.
- [51] M. Murdoch, G.I.N. Waterhouse, M.A. Nadeem, J.B. Metson, M.A. Keane, R.F. Howe, J. Llorca, H. Idriss, Nat. Chem. 3 (2011) 489–492.
- [52] J.G. Yu, J.F. Xiong, B. Cheng, S.W. Liu, Appl. Catal. B-Environ. 60 (2005) 211–221.
- [53] W.B. Hou, S.B. Cronin, Adv. Funct. Mater. 23 (2013) 1612–1619.
- [54] A. Tanaka, S. Sakaguchi, K. Hashimoto, H. Komami, ACS Catal. 3 (2013) 79–85.
- [55] J. Ke, J. Liu, H. Sun, H. Zhang, X. Duan, P. Liang, X. Li, M.O. Tade, S. Liu, S. Wang, Appl. Catal. B-Environ. 200 (2017) 47–55.
- [56] H. Li, Z.B. Xia, J.Q. Chen, L. Lei, J.H. Xing, Appl. Catal. B-Environ. 168 (2015) 105–113.
- [57] K. Zhao, X.Q. Yan, Y.S. Gu, Z. Kang, Z.M. Bai, S.Y. Cao, Y.C. Liu, X.H. Zhang, Y. Zhang, Small 12 (2016) 245–251.
- [58] D.M. Han, Z.Y. Ma, W.W. Zhao, J.J. Xu, H.Y. Chen, Electrochim. commun. 35 (2013) 38–41.
- [59] P.P. Wang, L. Cao, Y. Wu, J.W. Di, Microchim. Acta 185 (2018) 356.
- [60] H. Li, Y. Qiao, J. Li, H. Fang, D. Fan, W. Wang, Biosens. Bioelectron. 77 (2016) 378–384.
- [61] Y. Lin, Q. Zhou, D. Tang, Anal. Chem. 89 (2017) 11803–11810.
- [62] Y.F. Tang, Y. Chai, X.Q. Liu, L.L. Li, L.W. Yang, P.P. Liu, Y.M. Zhou, H.X. Ju, Y.Z. Cheng, Biosens. Bioelectron. 117 (2018) 224–231.

- [63] J. Yan, Z.G. Chen, H.Y. Ji, Z. Liu, X. Wang, Y.G. Xu, X.J. She, L.Y. Huang, L. Xu, H. Xu, H.M. Li, *Chem. Eur. J.* 22 (2016) 4764–4773.
- [64] J. Tian, Y. Li, J. Dong, M. Huang, J. Lu, *Biosens. Bioelectron.* 110 (2018) 1–7.
- [65] B.H. Fu, Z.H. Zhang, *Small* 14 (2018) 1703610.
- [66] I. Ibrahim, H.N. Lim, O.K. Abou-Zied, N.M. Huang, P. Estrela, A. Pandikumar, *J. Phys. Chem. C* 120 (2016) 22202–22214.
- [67] H.J. Shi, Y.L. Wang, J.Z. Zhao, X.R. Huang, G.H. Zhao, *J. Hazard. Mater.* 342 (2018) 131–138.
- [68] S. Chen, H. Nan, X. Zhang, Y. Yan, Z. Zhou, Y. Zhang, K. Wang, *J. Mater. Chem. B Mater. Biol. Med.* 5 (2017) 3718–3727.
- [69] M.C. Liu, X. Ding, Q.W. Yang, Y. Wang, G.H. Zhao, N.J. Yang, *J. Hazard. Mater.* 331 (2017) 309–320.
- [70] D. Jiang, X. Du, D. Chen, L. Zhou, W. Chen, Y. Li, N. Hao, J. Qian, Q. Liu, K. Wang, *Biosens. Bioelectron.* 83 (2016) 149–155.
- [71] X. Li, Z. Zheng, X. Liu, S. Zhao, S. Liu, *Biosens. Bioelectron.* 64 (2015) 1–5.
- [72] B. Zhang, H.Y. Meng, X. Wang, H.H. Chang, W.L. Wei, *Sens. Actuators B-Chem.* 253 (2017) 495–501.
- [73] G. Aragay, J. Pons, A. Merkoci, *Chem. Rev.* 111 (2011) 3433–3458.
- [74] N. Hildebrandt, C.M. Spillmann, W.R. Algar, T. Pons, M.H. Stewart, E. Oh, K. Susumu, S.A. Diaz, J.B. Delehanity, I.L. Medintz, *Chem. Rev.* 117 (2017) 536–711.
- [75] Z. Yue, F. Lisdat, W.J. Parak, S.G. Hickey, L.P. Tu, N. Sabir, D. Dorfs, N.C. Bigall, *ACS Appl. Mater. Interfaces* 5 (2013) 2800–2814.
- [76] G. Wen, X. Wen, M.M.F. Choi, S. Shuang, *Sens. Actuators B-Chem.* 221 (2015) 1449–1454.
- [77] G.L. Wang, K.L. Liu, Y.M. Dong, Z.J. Li, C. Zhang, *Anal. Chim. Acta* 827 (2014) 34–39.
- [78] Y. Zhang, A. Shoaib, J. Li, M. Ji, J. Liu, M. Xu, B. Tong, J. Zhang, Q. Wei, *Biosens. Bioelectron.* 79 (2016) 866–873.
- [79] W.W. Zhao, J.J. Xu, H.Y. Chen, *TrAC Trends Anal. Chem.* 82 (2016) 307–315.
- [80] L. Shi, Z. Chu, Y. Liu, J. Peng, W. Jin, *J. Mater. Chem. B Mater. Biol. Med.* 2 (2014) 2658–2665.
- [81] A.B. Iliuk, L.H. Hu, W.A. Tao, *Anal. Chem.* 83 (2011) 4440–4452.
- [82] L. Shi, X. Rong, Y. Wang, S. Ding, W. Tang, *Biosens. Bioelectron.* 102 (2018) 41–48.
- [83] Z.Y. Ma, J.B. Pan, C.Y. Lu, W.W. Zhao, J.J. Xu, H.Y. Chen, *Chem. Commun. (Camb.)* 50 (2014) 12088–12090.
- [84] H. Li, Y. Xue, W. Wang, *Biosens. Bioelectron.* 54 (2014) 317–322.
- [85] X.S. Wu, M. Sprinkle, X.B. Li, F. Ming, C. Berger, W.A. de Heer, *Phys. Rev. Lett.* 101 (2008) 026801.
- [86] Y.S. Shi, G.Q. Zhang, J.J. Li, Y. Zhang, Y.B. Yu, Q. Wei, *Microchim. Acta* 184 (2017) 1379–1387.
- [87] R. Ganatra, Q. Zhang, *ACS Nano* 8 (2014) 4074–4099.
- [88] D. Han, L. Jiang, W. Tang, J. Xu, H. Chen, *Electrochim. commun.* 51 (2015) 72–75.
- [89] M. Zhao, G.C. Fan, J.J. Chen, J.J. Shi, J.J. Zhu, *Anal. Chem.* 87 (2015) 12340–12347.
- [90] L. Shi, Z. Chu, X. Dong, W. Jin, E. Dempsey, *Nanoscale* 5 (2013) 10219–10225.
- [91] J. Tang, B. Kong, Y. Wang, M. Xu, Y. Wang, H. Wu, G. Zheng, *Nano Lett.* 13 (2013) 5350–5354.
- [92] L. Shi, Y. Wang, Z. Chu, Y. Yin, D. Jiang, J. Luo, S. Ding, W. Jin, *J. Mater. Chem. B Mater. Biol. Med.* 5 (2017) 1073–1080.
- [93] L. Shi, Z. Chu, Y. Liu, W. Jin, *J. Mater. Chem. B Mater. Biol. Med.* 3 (2015) 3134–3140.
- [94] S.P. Li, X.Q. Gu, Y.L. Zhao, Y.H. Qiang, S. Zhang, *J. Mater. Sci. Mater. Electron.* 27 (2016) 8455–8463.
- [95] Y.P. Luo, C. Dong, X.G. Li, Y. Tian, *J. Electroanal. Chem. Lausanne* (Lausanne) 759 (2015) 51–54.
- [96] X.M. Qu, F. Yang, H. Chen, J. Li, H.B. Zhang, G.J. Zhang, L. Li, L.H. Wang, S.P. Song, Y. Tian, H. Pei, *ACS Appl. Mater. Interfaces* 9 (2017) 16026–16034.
- [97] B.F. Ye, Y.J. Zhao, Y. Cheng, T.T. Li, Z.Y. Xie, X.W. Zhao, Z.Z. Gu, *Nanoscale* 4 (2012) 5998–6003.
- [98] G.L. Wang, T.T. Gu, Y.M. Dong, X.M. Wu, Z.J. Li, *Electrochim. commun.* 61 (2015) 117–120.
- [99] Y. Zang, J.P. Lei, Q. Hao, H.X. Ju, *ACS Appl. Mater. Interfaces* 6 (2014) 15991–15997.
- [100] J.W. Liu, Y. Lu, *J. Am. Chem. Soc.* 126 (2004) 12298–12305.
- [101] J. Liu, Y. Lu, *J. Am. Chem. Soc.* 129 (2007) 9838–9839.
- [102] W.B. Liang, Y. Zhuo, Y.N. Zheng, C.Y. Xiong, Y.Q. Chai, R. Yuan, *ACS Appl. Mater. Interfaces* 9 (2017) 39812–39820.
- [103] C. Zhang, Y.F. Zhi, *Chem. Mater.* 17 (2005) 3537–3545.
- [104] B. Zhang, L. Lu, Q. Hu, F. Huang, Z. Lin, *Biosens. Bioelectron.* 56 (2014) 243–249.
- [105] B. Zhang, L. Guo, *Biosens. Bioelectron.* 37 (2012) 112–115.
- [106] L.M. Gaetke, C.K. Chow, *Toxicology* 189 (2003) 147–163.
- [107] G.L. Wang, J.J. Xu, H.Y. Chen, *Nanoscale* 2 (2010) 1112–1114.
- [108] P. Wang, X.Y. Ma, M.Q. Su, Q. Hao, J.P. Lei, H.X. Ju, *Chem. Commun. (Camb.)* 48 (2012) 10216–10218.
- [109] F. Huang, F. Pu, X. Lu, H. Zhang, Y. Xia, W. Huang, Z. Li, *Sens. Actuators B-Chem.* 183 (2013) 601–607.
- [110] I. Ibrahim, H.N. Lim, N.M. Huang, A. Pandikumar, *PLoS One* 11 (2016) e0154557.
- [111] J.J. Yan, K. Wang, Q. Liu, J. Qian, X.Y. Dong, W. Liu, B.J. Qiu, *RSC Adv.* 3 (2013) 14451–14457.
- [112] Q.M. Shen, X.M. Zhao, S.W. Zhou, W.H. Hou, J.J. Zhu, *J. Phys. Chem. C* 115 (2011) 17958–17964.
- [113] H.F. Cheng, B.B. Huang, Y. Dai, *Nanoscale* 6 (2014) 2009–2026.
- [114] Y.X. Qiu, J. Li, H.B. Li, Q. Zhao, H.M. Wang, H.L. Fang, D.H. Fan, W. Wang, *Sens. Actuators B-Chem.* 208 (2015) 485–490.
- [115] Z. Kang, X.Q. Yan, Y.F. Wang, Z.M. Bai, Y.C. Liu, Z. Zhang, P. Lin, X.H. Zhang, H.G. Yuan, X.J. Zhang, Y. Zhang, *Sci. Rep.* 5 (2015) 7882.
- [116] Y.H. Zhu, Z.W. Xu, K. Yan, H.B. Zhao, J.D. Zhang, *ACS Appl. Mater. Interfaces* 9 (2017) 40452–40460.
- [117] H. Li, J. Li, D. Chen, Y. Qiu, W. Wang, *Sens. Actuators B-Chem.* 220 (2015) 441–447.
- [118] X.D. Zhang, X. Xie, H. Wang, J.J. Zhang, B.C. Pan, Y. Xie, *J. Am. Chem. Soc.* 135 (2013) 18–21.
- [119] Y.B. Li, H.M. Zhang, P.R. Liu, D. Wang, Y. Li, H.J. Zhao, *Small* 9 (2013) 3336–3344.
- [120] H. Sun, G. Zhou, Y. Wang, A. Suvorova, S. Wang, *ACS Appl. Mater. Interfaces* 6 (2014) 16745–16754.
- [121] S. Liu, J. Ke, H. Sun, J. Liu, M.O. Tade, S. Wang, *Appl. Catal. B-Environ.* 204 (2017) 358–364.
- [122] Q. Liu, T.X. Chen, Y.R. Guo, Z.G. Zhang, X.M. Fang, *Appl. Catal. B-Environ.* 193 (2016) 248–258.
- [123] P. Niu, L.L. Zhang, G. Liu, H.M. Cheng, *Adv. Funct. Mater.* 22 (2012) 4763–4770.
- [124] X. She, H. Xu, Y. Xu, J. Yan, J. Xia, L. Xu, Y. Song, Y. Jiang, Q. Zhang, H. Li, *J. Mater. Chem. A Mater. Energy Sustain.* 2 (2014) 2563–2570.
- [125] L. Xu, J.X. Xia, L.G. Wang, H.Y. Ji, J. Qian, H. Xu, K. Wang, H.M. Li, *Eur. J. Inorg. Chem.* (2014) 3665–3673.
- [126] B. Dhal, H.N. Thatoi, N.N. Das, B.D. Pandey, *J. Hazard. Mater.* 250 (2013) 272–291.
- [127] H. Li, J. Li, W. Wang, Z. Yang, Q. Xu, X. Hu, *Analyst* 138 (2013) 1167–1173.
- [128] R.S. Moakhar, G.K.L. Goh, A. Dolati, M. Ghorbani, *Appl. Catal. B-Environ.* 201 (2017) 411–418.
- [129] R.S. Moakhar, G.K.L. Goh, A. Dolati, M. Ghorbani, *Electrochim. commun.* 61 (2015) 110–113.
- [130] J. Luo, J. Sun, J. Huang, X.Y. Liu, *Chem. Eng. J.* 283 (2016) 1118–1126.
- [131] J. Luo, Q. Ma, W. Wei, Y. Zhu, R. Liu, X.Y. Liu, *ACS Appl. Mater. Interfaces* 8 (2016) 21028–21038.
- [132] J.Q. Fu, L.X. Chen, J.H. Li, Z. Zhang, *J. Mater. Chem. A Mater. Energy Sustain.* 3 (2015) 13598–13627.
- [133] L. Chen, S. Xu, J. Li, *Chem. Soc. Rev.* 40 (2011) 2922–2942.
- [134] T. Fang, X. Yang, L. Zhang, J. Gong, *J. Hazard. Mater.* 312 (2016) 106–113.
- [135] Y. Liang, B. Kong, A. Zhu, Z. Wang, Y. Tian, *Chem. Commun. (Camb.)* 48 (2012) 245–247.
- [136] R. Wang, X. Pang, H. Zhang, P. Gao, B. Du, H. Ma, Q. Wei, *Anal. Methods* 7 (2015) 5406–5411.
- [137] Y. Zhang, H. Ma, D. Wu, R. Li, X. Wang, Y. Wang, W. Zhu, Q. Wei, B. Du, *Biosens. Bioelectron.* 77 (2016) 936–941.
- [138] W.Y. Zhang, A.M. Asiri, D.L. Liu, D. Du, Y.H. Lin, *TrAC Trends Anal. Chem.* 54 (2014) 1–10.
- [139] H. Li, J. Li, Q. Xu, X. Hu, *Anal. Chem.* 83 (2011) 9681–9686.
- [140] H. Li, J. Li, Z. Yang, Q. Xu, X. Hu, *Anal. Chem.* 83 (2011) 5290–5295.
- [141] D. Jiang, X. Du, D. Chen, Y. Li, N. Hao, J. Qian, H. Zhong, T. You, K. Wang, *Carbon* 102 (2016) 10–17.
- [142] H. Wang, B. Zhang, F. Zhao, B. Zeng, *ACS Appl. Mater. Interfaces* 10 (2018) 35281–35288.
- [143] H. Li, J. Li, Q. Xu, Z. Yang, X. Hu, *Anal. Chim. Acta* 766 (2013) 47–52.
- [144] Q. Liu, J. Cai, J. Huan, X. Dong, C. Wang, B. Qiu, K. Wang, *Analyst* 139 (2014) 1121–1126.
- [145] H.P. Mao, Y.T. Yan, N. Hao, Q. Liu, J. Qian, S.B. Chen, K. Wang, *Sens. Actuators B-Chem.* 238 (2017) 239–248.
- [146] J. Song, S. Wu, P.P. Xing, Y.Q. Zhao, J.L. Yuan, *Anal. Chim. Acta* 1001 (2018) 24–31.
- [147] P.P. Wang, W.J. Dai, L. Ge, M. Yan, S.G. Ge, J.H. Yu, *Analyst* 138 (2013) 939–945.
- [148] C.J. Zhang, S.H. Si, Z.P. Yang, *Sens. Actuators B-Chem.* 211 (2015) 206–212.
- [149] Y. Wang, D. Zang, S. Ge, L. Ge, J. Yu, M. Yan, *Electrochim. Acta* 107 (2013) 147–154.
- [150] Y. Yan, H. Li, Q. Liu, N. Hao, H. Mao, K. Wang, *Sens. Actuators B-Chem.* 251 (2017) 99–107.
- [151] Q. Liu, J. Huan, X. Dong, J. Qian, N. Hao, T. You, H. Mao, K. Wang, *Sens. Actuators B-Chem.* 235 (2016) 647–654.
- [152] L. Shi, Y. Li, X. Rong, Y. Wang, S. Ding, *Anal. Chim. Acta* 968 (2017) 21–29.
- [153] D. Du, S. Chen, J. Cai, A. Zhang, *Biosens. Bioelectron.* 23 (2007) 130–134.
- [154] G.D. Liu, Y.H. Lin, *Anal. Chem.* 78 (2006) 835–843.
- [155] J. Gong, X. Wang, X. Li, K. Wang, *Biosens. Bioelectron.* 38 (2012) 43–49.
- [156] X. Sun, C. Gao, L. Zhang, M. Yan, J. Yu, S. Ge, *Sens. Actuators B-Chem.* 251 (2017) 1–8.
- [157] I.S. Cho, Z.B. Chen, A.J. Forman, D.R. Kim, P.M. Rao, T.F. Jaramillo, X.L. Zheng, *Nano Lett.* 11 (2011) 4978–4984.
- [158] P. Wang, G. Sun, L. Ge, S. Ge, J. Yu, M. Yan, *Analyst* 138 (2013) 4802–4811.
- [159] L. Ge, S.M. Wang, J.H. Yu, N.Q. Li, S.G. Ge, M. Yan, *Adv. Funct. Mater.* 23 (2013) 3115–3123.
- [160] S. Su, C. Zhang, L.H. Yuwen, J. Chao, X.L. Zuo, X.F. Liu, C.Y. Song, C.H. Fan, L.H. Wang, *ACS Appl. Mater. Interfaces* 6 (2014) 18735–18741.
- [161] F.K. Ma, Y.Z. Wu, Y.L. Shao, Y.Y. Zhong, J.X. Lv, X.P. Hao, *Nano Energy* 27 (2016) 466–474.
- [162] O. Lopez-Sanchez, D. Lembke, M. Kayci, A. Radenovic, A. Kis, *Nat. Nanotechnol.* 8 (2013) 497–501.
- [163] C.C. Wu, D. Jariwala, V.K. Sangwan, T.J. Marks, M.C. Hersam, L.J. Lauhon, *J. Phys. Chem. Lett.* 4 (2013) 2508–2513.
- [164] D. Jiang, X. Du, L. Zhou, H. Li, K. Wang, *Anal. Chem.* 89 (2017) 4525–4531.
- [165] M.E. van Apeldoorn, H.P. van Egmond, G.J.A. Speijers, G.J.I. Bakker, *Mol. Nutr.*

- Food Res. 51 (2007) 7–60.
- [166] J.W. Bennett, M. Klich, Clin. Microbiol. Rev. 16 (2003) 497–516.
- [167] K. Chen, M. Liu, G. Zhao, H. Shi, L. Fan, S. Zhao, Environ. Sci. Technol. 46 (2012) 11955–11961.
- [168] X. Du, D. Jiang, L. Dai, L. Zhou, N. Hao, J. Qian, B. Qiu, K. Wang, Biosens. Bioelectron. 81 (2016) 242–248.
- [169] Q. Liu, J. Huan, N. Hao, J. Qian, H. Mao, K. Wang, ACS Appl. Mater. Interfaces 9 (2017) 18369–18376.
- [170] V. Mani, B.V. Chikkaveeraiah, V. Patel, J.S. Gutkind, J.F. Rusling, ACS Nano 3 (2009) 585–594.
- [171] M.L. Ren, H.Y. Xu, X.L. Huang, M. Kuang, Y.H. Xiong, H. Xu, Y. Xu, H.Y. Chen, A. Wang, ACS Appl. Mater. Interfaces 6 (2014) 14215–14222.
- [172] Y. Lin, Q. Zhou, D. Tang, R. Niessner, H. Yang, D. Knopp, Anal. Chem. 88 (2016) 7858–7866.
- [173] J. Yang, P. Gao, Y. Liu, R. Li, H. Ma, B. Du, Q. Wei, Biosens. Bioelectron. 64 (2015) 13–18.
- [174] J. Tian, H. Zhao, H. Zhao, X. Quan, Microchim. Acta 179 (2012) 163–170.
- [175] A. Qileng, Y. Cai, J. Wei, H.T. Lei, W.P. Liu, S.S. Zhang, Y.J. Liu, Sens. Actuators B-Chem. 254 (2018) 727–735.
- [176] J. Wei, A.R. Qileng, Y. Yan, H.T. Lei, S.S. Zhang, W.P. Liu, Y.J. Liu, Anal. Chim. Acta 994 (2017) 82–91.
- [177] J. Feng, Y. Li, Z. Gao, H. Lv, X. Zhang, D. Fan, Q. Wei, Biosens. Bioelectron. 99 (2018) 14–20.
- [178] J. Tian, H. Zhao, X. Quan, Y. Zhang, H. Yu, S. Chen, Sens. Actuators B-Chem. 196 (2014) 532–538.
- [179] I. Oh, J. Kye, S. Hwang, Nano Lett. 12 (2012) 298–302.
- [180] R. Parameswaran, J.L. Carvalho-de-Souza, Y.W. Jiang, M.J. Burke, J.F. Zimmerman, K. Koehler, A.W. Phillips, J. Yi, E.J. Adams, F. Bezanilla, B.Z. Tian, Nat. Nanotechnol. 13 (2018) 260–266.
- [181] Y. Lin, Q. Zhou, D. Tang, R. Niessner, D. Knopp, Anal. Chem. 89 (2017) 5637–5645.
- [182] L.N. Vandenberg, I. Chahoud, J.J. Heindel, V. Padmanabhan, F.J.R. Paumgartten, G. Schoenfelder, Environ. Health Perspect. 118 (2010) 1055–1070.
- [183] L. Hu, C.C. Fong, X. Zhang, L.L. Chan, P.K.S. Lam, P.K. Chu, K.-Y. Wong, M. Yang, Environ. Sci. Technol. 50 (2016) 4430–4438.
- [184] W.G. Ma, L.N. Wang, N. Zhang, D.X. Han, X.D. Dong, L. Niu, Anal. Chem. 87 (2015) 4844–4850.
- [185] Y. Qiao, J. Li, H. Li, H. Fang, D. Fan, W. Wang, Biosens. Bioelectron. 86 (2016) 315–320.
- [186] Y. Wang, F. Chen, X. Ye, T. Wu, K. Wu, C. Li, Sens. Actuators B-Chem. 245 (2017) 205–212.
- [187] G. Sun, P. Wang, S. Ge, L. Ge, J. Yu, M. Yan, Biosens. Bioelectron. 56 (2014) 97–103.
- [188] Y. Hu, Z. Xue, H. He, R. Ai, X. Liu, X. Lu, Biosens. Bioelectron. 47 (2013) 45–49.
- [189] N. Hao, S.B. Chen, J. Qian, Y. Zhang, Q. Liu, X. Zhang, K. Wang, J. Electroanal. Chem. 801 (2017) 410–415.
- [190] L. Dai, X. Du, D. Jiang, W. Chen, M. Zhu, K. Wang, Microchim. Acta 184 (2017) 137–145.
- [191] H. Xie, K.Y. Duan, M.Y. Xue, Y.L. Du, C.M. Wang, Analyst 141 (2016) 4772–4781.
- [192] L. Xu, P. Yan, H. Li, S. Ling, J. Xia, Q. Xu, J. Qiu, H. Li, RSC Adv. 7 (2017) 7929–7935.
- [193] L. Xu, S. Ling, H. Li, P. Yan, J. Xia, J. Qiu, K. Wang, H. Li, S. Yuan, Sens. Actuators B-Chem. 240 (2017) 308–314.
- [194] Y. Liu, J. Jiang, Y. Sun, S. Wu, Y. Cao, W. Gong, J. Zou, RSC Adv. 7 (2017) 36015–36020.
- [195] P. Yan, L. Xu, J. Xia, Y. Huang, J. Qiu, Q. Xu, Q. Zhang, H. Li, Talanta 156 (2016) 257–264.
- [196] B. Zhang, L. Lu, F. Huang, Z. Lin, Anal. Chim. Acta 887 (2015) 59–66.
- [197] B.J. Lu, M.C. Liu, H.J. Shi, X.F. Huang, G.H. Zhao, Electroanalysis 25 (2013) 771–779.
- [198] R. Wang, K. Yan, F. Wang, J. Zhang, Electrochim. Acta 121 (2014) 102–108.
- [199] Q. Kang, L. Yang, Y. Chen, S. Luo, L. Wen, Q. Cai, S. Yao, Anal. Chem. 82 (2010) 9749–9754.
- [200] K. Yan, R. Wang, J. Zhang, Biosens. Bioelectron. 53 (2014) 301–304.
- [201] L. Zhou, D. Jiang, X. Du, D. Chen, J. Qian, Q. Liu, N. Hao, K. Wang, J. Mater. Chem. B 4 (2016) 6249–6257.
- [202] Y. Liu, R. Wang, Y. Zhu, R. Li, J. Zhang, Sens. Actuators B-Chem. 210 (2015) 355–361.
- [203] F. Baquero, J.-L. Martinez, R. Canton, Curr. Opin. Biotechnol. 19 (2008) 260–265.
- [204] P. Yan, D. Jiang, Y. Tian, L. Xu, J. Qian, H. Li, J. Xia, H. Li, Biosens. Bioelectron. 111 (2018) 74–81.
- [205] Y. Liu, K. Yan, J.D. Zhang, ACS Appl. Mater. Interfaces 8 (2016) 28255–28264.
- [206] Y. Liu, H. Zhang, J. Ke, J. Zhang, W. Tian, X. Xu, X. Duan, H. Sun, M.O. Tade, S. Wang, Appl. Catal. B-Environ. 228 (2018) 64–74.
- [207] H. Zhang, W. Tian, L. Zhou, H. Sun, M. Tade, S. Wang, Appl. Catal. B-Environ. 223 (2018) 2–9.
- [208] Y. Liu, K. Yan, O.K. Okoth, J. Zhang, Biosens. Bioelectron. 74 (2015) 1016–1021.
- [209] H. Li, J. Li, Y. Qiao, H. Fang, D. Fan, W. Wang, Sens. Actuators B-Chem. 243 (2017) 1027–1033.
- [210] A. Nezami, R. Nosrati, B. Golichenari, R. Rezaee, G.I. Chatzidakis, A.M. Tsatsakis, G. Karimi, TrAC Trends Anal. Chem. 94 (2017) 95–105.
- [211] L. Fan, G. Zhao, H. Shi, M. Liu, Y. Wang, H. Ke, Environ. Sci. Technol. 48 (2014) 5754–5761.
- [212] P.P. Liu, X.Q. Liu, X.H. Huo, Y.F. Tang, J. Xu, H.X. Ju, ACS Appl. Mater. Interfaces 9 (2017) 27185–27192.
- [213] X.J. Du, L.M. Dai, D. Jiang, H.N. Li, N. Hao, T.Y. You, H. Mao, K. Wang, Biosens. Bioelectron. 91 (2017) 706–713.
- [214] E. Thimsen, F. Le Formal, M. Gratzel, S.C. Warren, Nano Lett. 11 (2011) 35–43.
- [215] L. Feng, Z. Bian, J. Peng, F. Jiang, G. Yang, Y. Zhu, D. Yang, L. Jiang, J. Zhu, Anal. Chem. 84 (2012) 7810–7815.
- [216] J. Peng, L.-N. Feng, Z.-J. Ren, L.-P. Jiang, J.-J. Zhu, Small 7 (2011) 2921–2928.
- [217] R.X. Li, Y.X. Liu, T. Yan, Y.Y. Li, W. Cao, Q. Wei, B. Du, Biosens. Bioelectron. 66 (2015) 596–602.
- [218] H. Shi, J. Zhao, Y. Wang, G. Zhao, Biosens. Bioelectron. 81 (2016) 503–509.
- [219] Y.H. Zhu, K. Yan, Y. Liu, J.D. Zhang, Anal. Chim. Acta 884 (2015) 29–36.
- [220] H. Dai, S. Zhang, Z. Hong, X. Li, G. Xu, Y. Lin, G. Chen, Anal. Chem. 86 (2014) 6418–6424.
- [221] J. Gong, T. Fang, D. Peng, A. Li, L. Zhang, Biosens. Bioelectron. 73 (2015) 256–263.
- [222] J. Cai, P. Sheng, L. Zhou, L. Shi, N. Wang, Q. Cai, Biosens. Bioelectron. 50 (2013) 66–71.
- [223] R. Hallaj, N. Haghighi, Microchim. Acta 184 (2017) 3581–3590.
- [224] F.W.P. Ribeiro, F.C. Moraes, E.C. Pereira, F. Marken, L.H. Mascaro, Electrochim. Commun. 61 (2015) 1–4.
- [225] N. Muthuchamy, K.P. Lee, A.I. Gopalan, Biosens. Bioelectron. 89 (2017) 390–399.
- [226] L. Shi, Z. Chu, Y. Liu, W. Jin, N. Xu, Adv. Funct. Mater. 24 (2014) 7032–7041.
- [227] Z.P. Chen, W.C. Ren, L.B. Gao, B.L. Liu, S.F. Pei, H.M. Cheng, Nat. Mater. 10 (2011) 424–428.
- [228] M. Ongaro, M. Signoretto, V. Trevisan, A.M. Stortini, P. Ugo, Chemosensors 3 (2015) 146–156.
- [229] R. Ojani, S. Safshekan, J.B. Raoof, J. Solid State Electrochem. 18 (2014) 779–783.
- [230] Y. Su, S. Yang, W. Liu, L. Qiao, J. Yan, Y. Liu, S. Zhang, Y. Fang, Microchim. Acta 184 (2017) 4065–4072.